EXPERIMENTAL STUDY OF BEAMS WITH WEB OPENINGS

by

KUO-SHU CHENG

Diploma, Taipei Institute of Technology,
Taiwan, China, 1965

A MASTER'S THESIS

submitted in partial fulfillment of the

requirements for the degree

MASTER OF SCIENCE

Department of Civil Engineering

KANSAS STATE UNIVERSITY
Manhattan, Kansas

1969

Approved by:

Peter B Cooper
Major Professor

TABLE OF CONTENTS

LIST OF TABLES

Tables

LIST OF FIGURES

LIST OF FIGURES (cont.)

INTRODUCTION

1. Introduction

In the construction of buildings, ship bulkheads, and aircraft, holes through the webs of structural members are frequently necessary for the passage of pipes, electric cables, ventilation ducts, and for other purposes. In the past few years, web openings in beams have been studied by several researchers; however, additional data on the stress distribution adjacent to the hole is still needed. The purpose of the study described in this thesis was to investigate the effect of a rectangular hole with round corners on the elastic stresses in a wide-flange beam subjected to combined bending and shear.

The photostress method in conjunction with electrical resistance strain gages was used for experimental measurements in the investigation. The so-called Vierendeel Method was used to calculate theoretical stresses around the hole in the web.

2. Objectives

The objectives of this investigation were:

1. To compare the results of experimental stress analysis around the hole using the Photoelastic Method and electrical resistance strain gages with predictions based on the Vierendeel Method of analysis.

2. To study the effect of the web opening on beam deflections in the elastic and inelastic ranges.

3. Scope

This study was limited to tests on an 8 in. deep A36 steel WF beam with a weight of 35 lbs. per foot (8 WF 35). Elastic strains were measured around the periphery of the opening and over the adjacent regions of the web. Two rectangular openings, located at the 1/4 point of the span, were tested. Both openings were unreinforced and were centered on the centroidal axis of the beam. The corners of the opening were rounded with a radius of 1/2".

In testing the beam, simple supports were used at the end and a concentrated load was applied at the center of the span. After elastic stress had been measured, the specimen was subjected to an ultimate load test.

LITERATURE SURVEY

1. Analytical Solutions

In 1932, Muskhelishvili[1] introduced several methods to develop stress equations to solve elasticity problems based on the fundamentals of differential and integral calculus and on the elementary theory of functions of a complex variable.

Heller, Block and Bart[2], in 1962, investigated the stress around a rectangular opening with rounded corners in the web of a beam. This investigation was based on the complex variable method associated with Muskhelishvili and a conformal mapping technique. The effects of varying the corner radius and the aspect ratio of the opening (ratio of depth to width of opening) on the stress distribution in a beam were included in the study.

Bower[3], also using the theory of elasticity techniques associated with Muskhelishvili, investigated the stresses around an elliptical hole in a wide-flange beam subjected to a uniform loading. Although the analysis is similar to that of Heller et al., Bower's solution in addition permits stresses at any other point in the web to be determined. From this investigation, it was concluded that (1) the applicability of the analysis depends on the size of the web hole and the magnitude of the moment-shear ratio at the hole; (2) the stress distributions near elliptic holes in uniformly loaded beams are widely different in magnitude and in appearance from the distributions occurring in beams without holes; and

(3) the solution is valid for predicting stresses near the opening providing the opening depth does not exceed half the web depth.

In place of the theory of elasticity, the well-known "Vierendeel Analysis" has been used by design engineers to calculate the elastic stresses around rectangular holes in the webs of wide-flange beams.[4,5] This method can be applied to single rectangular opening or adjacent rectangular openings and is based on the assumption that points of contraflexure occur in the tee section above and below the opening on the opening center line. Bower has suggested that the Vierendeel Method is satisfactory for predicting bending stresses on the transverse cross-section of a beam with a rectangular opening but does not predict the stress concentrations near the corners.

2. Experimental Studies

Bower[4] has reported experimentally measured stresses in wide-flange beams with web openings. He made use of electrical resistance strain gages to determine these stresses in a series of tests on A36 steel wide-flange beams weighing 36 lbs. per ft. (16WF36). Rectangular and circular holes were studied with all holes centered on the centroid axis of the beam. All specimens were tested as simply supported beams and were loaded with one or two concentrated loads. Based on this investigation, it was concluded (1) the theoretical results based on the theory of elasticity and the Vierendeel Method are correct, and (2) the elasticity analysis is complex and requires a

computer solution, while the Vierendeel analysis is relatively simple to perform.

In an extensive program supported by the Canadian Institute of Steel Construction, researchers at McGill University have conducted a series of theoretical and experimental studies of web openings in beams.[5] Two beam sizes, ASTM A36 8WF17 and 14WF30, were used as specimens. The types of openings studied included rectangular holes (12" x 8"), circular holes (diameter 8") and eliptical holes 16" x 8"). Some of the conclusions can be summarized as follows: (1) Stress concentrations occur at the corners under all loading conditions. (2) Experimental studies verify that the Vierendeel Analysis is satisfactory and can be used to predict the stress around most of the rectangular opening at ultimate load. (3) For one or two circular openings deflections are greater than values estimated by ignoring the presence of the opening by about 10%. For one rectangular opening the calculated deflections are not more than 10-15% lower than the measured values.

In 1963, Segner[6] reported the results of a study of the requirements for reinforcement around large rectangular openings in the webs of wide-flange beams subjected to different combinations of bending moment and shear. From the tests, it was concluded that (1) large deflections should be expected when beams contain openings in the webs, but the deeper the beam is, the less deflection it has. (2) the Vierendeel Truss analogy is an appropriate method of analysis for such problems.

For beams with very deep holes or with long rectangular holes, local buckling should be considered in the design. Cato and McClellan[7], in 1964, conducted a few tests in which they studied the effect of the hole location relative to the supports on the strength of the shear panel between the support and the hole. It was observed that, for short panels, local crippling over the supports occurred. For longer shear panels neither crippling nor buckling occurred.

In 1966, Arora[8] completed an experimental stress analysis of an I-beam with a rectangular web cutout. Electrical resistance strain gages and photoelasticity techniques were used to determine stresses around the opening. From these tests, it was observed that (1) the elastic stress distribution obtained from the experimental results did not agree with the stresses computed on the basis of simple beam theory; (2) the neutral axis for the various sections of the beam did not coincide with the centroidal axis of the beam; (3) the photoelastic method of experimental stress analysis was found to be quite effective.

In 1961, Hendry and Shawki[9] studied the stresses in a deep beam with a central concentrated load. Their conclusions can be summarized in two parts: (1) The theoretical solutions are difficult where the loading is unsymmetrical or when there are holes in a beam. (2) In those cases the easiest solution is obtained by the photoelastic method.

EXPERIMENTAL PROGRAM

1. Introduction

The purpose of this investigation was to determine experimentally the stresses in a wide-flange beam with a web opening, and to compare these experimental stresses with those predicted by theory. The entire experimental program, including the determination of beam dimensions and physical properties, the design of the test program, the design of the test beam and set up, the instrumentation, and the test procedure, were planned to achieve this purpose.

2. Determination of Beam Dimensions and Physical Properties

It was anticipated that the actual dimensions of the wide-flange specimen would vary somewhat from the nominal dimensions, and that the actual physical properties would be different from the nominal values specified for ASTM A36 steel. For an accurate calculation of theoretical values of stresses and deflections, it was necessary to determine the actual cross-section dimensions and physical properties of the test beam.

In determining the actual cross-section dimensions, the beam was laid out in twelve sections as shown in Fig. 1. At each of these sections, the flange width and beam depth were measured. The thickness of the top and bottom flanges were measured at two points on each of the twelve cross sections, and the web thickness was determined at three points at each end of the beam. These measured dimensions are presented in

Table 1. The average values, also shown in the table, were used in all subsequent calculations.

For the purpose of determining the actual physical properties, six tensile coupons were taken from a section of the test beam after all tests had been completed. Two coupons were cut from each flange and two from the web of this section, as shown in Figure 2.

The dimensions of all the tensile coupons were based on ASTM standards for physical and mechanical testing of material[11] and are shown in Fig. 2. The coupon test results are listed in Table 2, and are compared with the nominal values in Table 3. A typical stress-strain diagram is shown in Fig. 3. The results indicate that the yield stress, ultimate tensile strength and the modulus of elasticity of the flanges were a little different from those of the web.

3. Test Program

The testing program was divided into four parts. Initially, for Case I, the beam was tested without a web opening. The deflections of the beam were recorded for 8 different loads, ranging from 0-16000 lbs. in 2000 lb. increments.

For Case II, a 2" x 4" opening with 1/2" radius rounded corners was cut in the web at the quarterpoint of the span. Loads were applied in 4000 lb. increments up to the maximum load of 16000 lbs. Strain gage, deflection and photostress readings were taken at each load.

For Case III, the opening was enlarged to 4" x 6" with the same size corner fillets as Case II. The same loading range and measuring procedures were employed as in Case II.

For Case IV, the beam was painted with a whitewash coating and was then subjected to an ultimate strength test.

4. Test Beam Fabrication

The experimental phase of this study was conducted on an ASTM A36 wide-flange beam having a depth of 8" and a weight of 35 lbs. per ft. (8WF35), with a rectangular opening in the web. For Case II, the rectangular opening in the web was cut to the dimensions of 2" x 6" at the quarterpoint of the span with the corners of the opening rounded with 1/2" fillet. The opening was fabricated by first using a high speed drill to drill 1" diameter holes at the four corners of the opening, then using a high speed vibrating saw to cut out the sides of the opening. The final finishing work was done with sand paper, polishing the rough sides of the opening and the web near the opening to facilitate the attachment of the strain gages and photostress coating.

5. Photostress Measurements

a. Principle of Photostress Measurements

The principal purpose of photostress measurements is to determine the direction, magnitude and sign of the principal strains at any point on the surface of a structural member. For this investigation, a large Field Meter (LF/M)

with its accessories was used to determine isoclinics and isochromatics from point to point for the purpose described above. The term "Isoclinic" is defined as a locus of points along which the directions of the principle strains are constant. "Isochromatic" is defined as a locus of points along which the magnitude of the principle strain difference is a constant.

b. General Procedure for Photostress Readings

The Large Field Meter consists of a polarizer and analyzer arranged so that the light from the polarizer strikes the photostress plastic sheet and is reflected back to the analyzer as shown in Fig. 4. The Analyzer consists of a quarter wave plate and an analyzer ring with a scale for measuring the isochromatics. The polarizer consists of a quarter wave plate which is coupled together with the analyzer so that they can be rotated simultaneously, and the different isoclinic angles can be read on the isoclinic scale. Fig. 5a illustrates the optical system used in this LF/M. The Quarter Wave Plate is not used in the system for setting the LF/M with plane polarized light (Fig. 5a), and the analyzer handle is rotated either clockwise or counterclockwise in order to produce an isoclinic which is parallel to the direction of principle strain ϵ_1 at a particular point of interest. The LF/M is then changed to circular polarized light (Fig. 5b) so that the isoclinics are removed, and isochromatic readings are recorded by rotating the analyzer ring either clockwise or counterclockwise until a fringe falls exactly on the same particular point.

c. Procedure for Fringe Order Between Zero and One

For the present case, since there was a large opening in the web, sufficient load could not be applied to develop a full fringe at many points on the plastic sheet. Therefore, the Full Wave Plate and Compensator were mounted on the analyzer Quarter Wave Plate. The Compensator was used to determine between which two fringes the point of interest lay and the full wave plate was used for analysis between zero and the first fringe. For using the Full Wave Plate and Compensator, it was necessary to note that the compensator and the Full Wave Plate were added only when the analyzer handle and the direction of the major principle stress were parallel. With the Compensator parallel to the direction of the major principle strain, a zero fringe should appear at the point of interest. Thus the compensator was used to distinguish whether the zero fringe appeared or not. If the zero fringe appeared, the analyzer handle was parallel to ε_1, otherwise it was not. If it was not parallel to ε_1, the analyzer handle was rotated clockwise or counterclockwise through 90° from its original position. After the direction of principle stress had been determined, an accurate measurement could be made by use of the Tardy Method.[8,15,16]

d. Preparation of Specimen

Budd Type S photostress sheet plastic was selected and cut to the required dimensions by using a special model making kit. Budd Photostress RCT (S&A) reflective cement, resin and hardener were used to fasten the plastic sheet to

the web of the beam. The bonding agent was poured and brushed uniformly on the web surface approximately 1/16" thick. Cellophane tape was used to hold the plastic sheet in position during curing, with no pressure being applied. The bonding was complete after 24 hours at a temperature of 75°F. Figure 6 shows the location of the plastic sheet on the web of test beam for Cases II and III.

6. Electrical Resistance Strain Gage Measurements

Budd Metal film C6-141-R3C, C6-141 and C6-141B gages, which are temperature compensated for steel, were used in this investigation. These gages were mounted at the locations shown in Figs. 7 and 8 with Eastman 910 cement. C6-141 and C6-141B gages were used to measure longitudinal strains, while the rosette gages (C6-161-R3C) were used to measure both longitudinal strains and shearing strains. Hooke's law was used to convert the strains to stresses using the values of the modulus of elasticity and Poisson's ratio given in Table 3. The strain gages were connected to a Budd Model A 110 D strain indicator used in conjunction with a Budd Model C-101-C switch and balance unit. An automatic printer was also used for facilitating the handling of the data.

7. Deflection Measurements

In Cases I, II, and III, dial gages with 1/2" stroke were used at the quarterpoints and midspan of the beam to measure deflections (see Fig. 9) in the elastic range. In Case IV, a dial gage with a 2" stroke was used at midspan to measure the

deflection from the elastic range until the ultimate load was attained. The locations of the dial gages for Cases I, II, and IV, are shown in Figs. 9 and 10.

8. Test Setup

For all the tests, the beam was loaded as a simple supported beam with one concentrated load at midspan. The load was applied through a steel block which was placed on the center line of the top flange. A 20 ton screw type testing machine was used to apply the load. The beam was aligned as closely as possible with the testing machine and supports so as to avoid any twisting. A sketch of the test set-up is shown in Fig. 9 and a photograph is shown in Fig. 10.

9. Test Procedure

After recording the readings of all the instruments at zero load, a load increment was applied and held while a second set of readings was taken and recorded. Additional load increments were applied and held for measurements until the maximum load of the test was reached. For Case IV, the test was continued into the inelastic range until the ultimate load was attained, with visual observations of the behavior of the beam and the mode of the failure being recorded during this portion of the test.

TEST RESULTS

1. Introduction

Figures 14 through 31 present graphically the data taken during the test program. An analysis of this data, which includes deflections, electrical resistance strain gage readings, and photostress readings, is presented in this section.

2. Deflections

a. Elastic Range

As shown in Figs. 9 and 10, the deflections were measured with 3 dial gages located at the quarter points and at midspan. The experimental and theoretical values of the deflections of the test beam without a web opening are given in Fig. 14 while those for Cases II and III (with an opening) are given in Figs. 15 and 16, respectively.

The theoretical elastic deflections were calculated using the following equations. Equation 1 was used to calculate the deflection of the test beam without the opening; Eq. 2 was used for the beam with an opening.

$$\delta = \int_{\ell} \frac{Mm}{EI}\,dx + \int_{\ell} k\,\frac{Vv}{AG}\,dx \qquad (1)$$

$$\delta = \int_{\ell-b} \frac{Mm}{EI}\,dx + \int_{b} \frac{Mm}{E(I-I_o)}\,dx + \int_{\ell-b} k\,\frac{Vv}{AG}\,dx + \int_{b} k\,\frac{Vv}{(A-A_o)G}\,dx \qquad (2)$$

where I = moment of inertia of the gross beam, I_o = moment of inertia of a section through the opening, A = area of the gross beam, and A_o = area of a section through the opening. All of these section properties were calculated from measured cross section dimensions. A value of E = 2.96 x 10^6 psi was obtained from the coupon tests, and a value of G = 11.15 x 10^6 psi was obtained by assuming Poisson's ratio μ = 0.3. In Eqs. 1 and 2, k is the shear shape factor and is approximately equal to the ratio of the total area to the web area for wide-flange beams.[12]

Comparing the theoretical and experimental deflections of Case I as shown in Fig. 14, it was found that the theoretical values calculated using Eq. 1 agreed quite well with the dial gage readings, with a 1% difference at midspan and a 0.5% difference at the quarter points. These small differences may be attributed to factors such as the web of the beam being slightly inclined, the two ends of the machine table bending slightly due to the applied load, or a small twisting stress developing due to slightly non-parallel flanges on the test beam.

The deflections for Cases II and III are shown in Figs. 15 and 16. The differences between the theoretical values calculated using Eq. 2 and the experimental data are summarized in Table 4. From the table, it can be seen that the deflections of a beam with a web opening are substantially larger than the beam without an opening. Since the experimental and theoretical deflections were in close agreement, it has been demonstrated

that Eq. 2 is a very good tool for determining the deflections of a beam with a large web opening in the elastic range.

b. Ultimate Load Test

Experimental and theoretical load deflection curves from the ultimate load test are given in Fig. 17. The theoretical curve was calculated using simple plastic theory[13] in the inelastic range and using Eq. 2 in the elastic range.

From Fig. 17, it is evident that the experimentally determined load-deflection curve is quite close to the idealized load deflection curve calculated by plastic theory. The theoretical ultimate load based on simple plastic theory and the yield point determined from the tensile coupon tests was 43.5 kips. The experimental value of the ultimate load at the beginning of the yield plateau was about 44.5 kips. As further deflection was imposed on the specimen, the load increased slightly, probably due to strain-hardening in the extreme fibers of the cross section. The ultimate load test was terminated when the midspan deflection was about five times the maximum elastic deflection.

3. Electrical Resistance Strain Gage Readings

The linear relationship between uniaxial stress and strain which exists within the elastic range of a material is well known. Hence, the bending and shearing stresses in the test beam could be determined experimentally by using strain gages oriented in the direction of the desired stresses. As previously mentioned, 12 Budd C6-141-B strain gages and 2

Budd C6-161-R3C rosette gages were used in the present investigation to investigate bending stresses along the vertical sections "0", "5", and "10", and shearing stresses along vertical section "5", as shown in Figs. 7 and 8.

The strain gage readings were recorded for four different load levels during the Case II and Case III tests. These readings are presented in Tables 5 and 6 for Cases II and III, respectively. Typical load-strain curves for one flange gage (No. 4) and one rosette (Gage Nos. 12, 13, and 14) are shown in Figs. 18 and 19 for the two cases. From these figures and other similar plots which are not shown here, it was found that all the strain gages yielded data which was linearly related to the applied load.

The normal bending stresses were calculated using Eq. 3 and are given in Table 7 for Case II and in Table 8 for Case III.

$$\sigma_x = E \cdot \varepsilon \tag{3}$$

where σ_x = normal bending stress; E = Young's modulus (29.6×10^3 ksi) and ε = strain gage reading.

For measuring shear stresses along vertical section "5", 2 Budd C6-141-R3C strain rosette gages were used with the three measuring grids arranged 120° apart. (See Figs. 7 and 8). In order to determine the shear strains, substitution of the data into the following general strain equation was necessary.

$$\varepsilon_n = \frac{\varepsilon_x+\varepsilon_y}{2} + \frac{\varepsilon_x-\varepsilon_y}{2} \cos 2\theta - \frac{\gamma_{xy}}{2} \sin 2\theta \tag{4}$$

Then, three sets of simultaneous equations could be obtained.

$$\varepsilon_a = \frac{\varepsilon_x+\varepsilon_y}{2} + \frac{\varepsilon_x-\varepsilon_y}{2}\cos 2\theta_a - \frac{\gamma_{xy}}{2}\sin 2\theta_a$$

$$\varepsilon_b = \frac{\varepsilon_x+\varepsilon_y}{2} + \frac{\varepsilon_x-\varepsilon_y}{2}\cos 2\theta_b - \frac{\gamma_{xy}}{2}\sin 2\theta_b \qquad (5a)$$

$$\varepsilon_c = \frac{\varepsilon_x+\varepsilon_y}{2} + \frac{\varepsilon_x-\varepsilon_y}{2}\cos 2\theta_c - \frac{\gamma_{xy}}{2}\sin 2\theta_c$$

For the present case, since the rosette strain gages are equiangular, $\theta_a = 180°$, $\theta_b = 60°$ and $\theta_c = 120°$. Solving Eqs. 5a using these values, ε_x, ε_y, γ_{xy} were obtained in terms of ε_a, ε_b, ε_c

$$\varepsilon_x = \varepsilon_a$$

$$\varepsilon_y = \frac{1}{3}(2\varepsilon_b + 2\varepsilon_c - \varepsilon_a) \qquad (5b)$$

$$\gamma_{xy} = \frac{2}{\sqrt{3}}(\varepsilon_c - \varepsilon_b)$$

The shear stresses were then computed by using

$$S_{xy} = \gamma_{xy} \cdot G \qquad (6)$$

where G is the modulus of rigidity ($G = 11.15 \times 10^3$ ksi). A typical calculation of the shear stress is given in the following example.

Example:

The No. 12-13-14 rosette gage was located 1/2 inch above the opening along vertical section "5" (see Fig. 7) and yielded the readings $\varepsilon_a = +104$, $\varepsilon_b = -78$, $\varepsilon_c = +308$ $(\frac{\text{Micro-inches}}{\text{inch}})$ due to a midspan load of 1600 lbs.

$\varepsilon_a = +104$ $\qquad$ $\theta_a = 180°$

$\varepsilon_b = -78$ $\qquad$ $\theta_b = 60°$

$\varepsilon_c = +308$ $\qquad$ $\theta_c = 120°$

$\varepsilon_x = \varepsilon_a = 104$ (micro-inches/inch)

$$\varepsilon_y = \frac{1}{3}[2(308-78)-104] = 119$$

$$\gamma_{xy} = \frac{2}{\sqrt{3}}[308-(-78)] = \frac{2 \times 286}{\sqrt{3}} = 446$$

For normal bending stresses

$$\sigma_x = E \cdot \varepsilon_x = 29.6 \times 10^6 \times 104 \times 10^{-6} = 3020 \text{ psi}$$

$$S_{xy} = \gamma_{xy} \cdot G = 446 \times 10^{-6} \times 11.15 \times 10^6 = 4980 \text{ psi}$$

The shear stresses along vertical section "5" calculated from Eqs. 5b and 6 were 4.12 ksi and 4.98 ksi for the rosettes located 1 1/2 in. and 1/2 in., respectively, above the opening of Case II. For Case III, the corresponding maximum shear

stress was 6.45 ksi for the rosette located 1/2 in. above the opening.

4. Photostress Readings

The photostress measurement techniques have been described previously. Calculations based on the "Shear difference method" are presented in this section. A general presentation and analysis of the data, including the correction of residual birefringence readings and the calibration of the Full Wave Plate, are also presented in this section.

(a) Calculation of One Fringe Value

The term "fringe value" in photoelasticity is defined as the magnitude of the principal strain difference $(\varepsilon_1-\varepsilon_2)$, or the principal stress difference required to produce a unit fringe on the photostress coating. From photoelasticity, it can be shown that the fringe order is[8,14]

$$N_n = \delta_n/\lambda \tag{7}$$

where λ is the wave length of light = 22.7×10^{-6} inches, and δ_n is the relative retardation which can be expressed as

$$\delta_n = 2\, t_p\, K\, C\, (\varepsilon_1 - \varepsilon_2) \tag{8}$$

In Eq. 8, t_p is the thickness of the photostress coating, K is the strain optical sensitivity constant of the photostress coating and C is the birefringence reinforcing factor.

Solving Eqs. 7 and 8, a new relationship between principle strain and the properties of the material is obtained.

$$(\varepsilon_1 - \varepsilon_2) = \lambda N_n / 2t_p K \cdot C \qquad (9a)$$

$$(\varepsilon_1 - \varepsilon_2) = f \cdot N_n \qquad (9b)$$

where f is the fringe value ($\frac{\lambda}{2t_p KC}$) and N_n is the fringe order (isochromatic reading).

For the present investigation, since a photostress coating of type S was selected, the properties of the material were given in Budd Bulletin BN 8002[15] and therefore:

t_p = .118 inches

K = .085

C was taken equal to 1, since there was no bending in the plane of the plastic sheet[8,15,17]. From Eqs. 9a and 9b,

$$f = \lambda / 2t_p \cdot K \cdot C$$

$$= (22.7 \times 10^{-6}) / 2 \times .118 \times .085$$

$$= 1200 \ \frac{\text{micro-inches}}{\text{inch}}$$

Assuming $N_n = 1$

$$(\varepsilon_1 - \varepsilon_2) = f \cdot N_n = 1200 \times 1 = 1200 \ \frac{\text{micro-inches}}{\text{inch}}$$

Converting this principle strain difference into a principle stress difference.

$$(\sigma_1 - \sigma_2) = (\varepsilon_1 - \varepsilon_2)E/(1+\mu) \qquad (10)$$

Assuming $\mu = 0.3$ (Poisson's ratio for steel) and using $E = 29.6 \times 10^3$ ksi from the tensile coupon tests,

$$(\sigma_1 - \sigma_2) = 1200 \times 10^{-6} \times 1296 \times 10^6)/(1+0.3)$$

$$= 27200 \text{ psi}$$

This means that 27.2×10^3 psi is required to produce one fringe of birefringence in the type S plastic sheet.

b. Calibration of Full Wave Plate

As described previously, sufficient load could not be applied to develop one fringe or more at most points on the photostress coating in the two test cases, since there was a large unreinforced opening in the web of the beam. Therefore, the Compensator and Full Wave Plate were needed to observe the birefringence between zero and the first fringe. However, the Full Wave Plate usually has some initial errors and must be calibrated with the compensator. The calibration procedure consists of two steps:

Step 1. Polish a very smooth surface along the opening and observe this uncoated reflective surface through the Full Wave Plate.

Step 2. Rotate the analyzer ring clockwise or counterclockwise until a purple color appears, called the tint of passage.

For the present case, the tint of passage appeared at a reading of .03 with a counterclockwise rotation of the analyzer

ring. Since all the isochromatic readings were measured with a clockwise rotation of the analyzer ring, all of these isochromatic readings were increased by .03.

c. Correction of Residual Birefringence Readings

Since some residual birefringence was present in the photostress coating, a zero load correction was necessary. With increases in the load, it was found that the isoclinics did not change much. Therefore, it was possible to add and subtract the zero load readings to obtain corrected readings. The birefringence readings at each point for four different loads were taken. A straight line graph was then drawn to see if the straight line passed through the origin. If the line did pass through the origin, there was no residual birefringence at that point; otherwise, a parallel straight line was drawn through the origin to correct for residual birefringence. Some of these graphs are shown in Fig. 20. The corrected isoclinic and isochromatic readings for each point in Cases II and III are given in Tables 9 and 10, respectively.

(d) Shear Difference Method[8,16]

A convenient method to determine the normal stresses at interior points on the web is the shear-difference method[8,16]. This method is based on the equations of equilibrium, which, when applied to the two dimensional stress problem, reduce to

$$\frac{\partial \sigma_x}{\partial x} + \frac{\partial S_{xy}}{\partial y} = 0 \qquad (11)$$

$$\frac{\partial \sigma_y}{\partial y} + \frac{\partial S_{xy}}{\partial x} = 0 \qquad (12)$$

Equation 11 can be integrated along the x-axis (Fig. 21), according to the relation

$$\int_o^x \frac{\partial \sigma_x}{\partial x}\, dx + \int_o^x \frac{\partial S_{xy}}{\partial y}\, dx = 0$$

This equation can be evaluated by applying the Finite-Difference Method, where the partial differences are replaced by the stress differences as shown below,

$$\int_o^{x_1} \frac{\partial \sigma_x}{\partial x}\, dx = (\sigma_x)_1 - (\sigma_x)_o$$

$$\int_o^{x_1} \frac{\partial S_{xy}}{\partial x}\, dx = \left[\frac{\Delta S_{xy}}{\Delta_y}\right]_{\frac{x_o+x_1}{2}} \cdot \Delta_x = \Sigma \frac{\Delta S_{xy}}{\Delta_y} \cdot \Delta_x$$

and therefore Eq. 11 can be formed as Eq. 13.

$$(\sigma_x)_1 = (\sigma_x)_o - \Sigma \frac{\Delta S_{xy}}{\Delta_y} \Delta_x \tag{13}$$

If the procedure is continued stepwise, as indicated in Eq. 13, all of the σ_x-values can be determined all along a line segment.

$$(\sigma_x)_1 = (\sigma_x)_o - \Sigma \frac{\Delta S_{xy}}{\Delta_y} \Delta_x$$

$$(\sigma_x)_2 = (\sigma_x)_1 - \Sigma \frac{\Delta S_{xy}}{\Delta_y} \Delta_x$$

$$(\sigma_x)_3 = (\sigma_x)_2 - \Sigma \frac{\Delta S_{xy}}{\Delta_y} \Delta_x$$

The value of the transverse stress, σ_y, for any point can be computed from Mohr's circles of stress (Figs. 22 and 23) and is given by the following equation:

$$\sigma_y = \sigma_x \pm \sqrt{(\sigma_1-\sigma_2)^2 - 4S_{xy}^2} \tag{14}$$

The normal bending stress at a point along any vertical section can also be found in a similar fashion by summing up forces in the vertical direction. Starting from any point along a horizontal section, and either going up or down from there, the transverse stress, σ_y, is given by

$$\sigma_y = (\sigma_y)_4 - \Sigma \frac{\Delta S_{xy}}{\Delta_x} \Delta_y \tag{15}$$

σ_x can also be obtained by applying Mohr's circle;

$$\sigma_x = \sigma_y \pm \sqrt{(\sigma_1-\sigma_2)^2 - 4S_{xy}^2} \tag{16}$$

From Fig. 22, the shear stress at any point in the two dimensional stress plane can be determined from Mohr's circle.

$$S_{xy} = \frac{1}{2}(\sigma_1 - \sigma_2) \sin 2\theta \tag{17}$$

In this investigation, the isochromatic readings, isoclinic angles and the properties of the photostress coating were punched on IBM cards, so that much of the stress calcula-

tion could be performed on the 1620 digital computer. The computer program used for determining the shear stresses and some of the quantities required for the normal stress calculations are shown in Appendix A. A sample of the input data for the computer program is given in Appendix Table A1, and a sample output is given in Table A2.

The procedures for calculating normal stresses σ_x and σ_y are described in greater detail in Ref. 8. For the present investigation, an example of the calculation of the normal stresses σ_x and σ_y, based on Eqs. 15 and 16, the procedures of calculation described in Ref. 8, and some data from the output of the computer program, are shown in Tables 11 and 12, for Case II, in Table 13 for Case III.

COMPARISON OF THE RESULTS AND DISCUSSION

Figures 24 through 31 present a comparison of the stresses obtained from the strain gage data, the photostress data and from a theoretical analysis based on the "Vierendeel Method", which is described in Appendix B.

The normal bending stresses, σ_x, along vertical section "0" are shown in Figs. 24 and 28 for Cases II and III, respectively. For the two cases, the strain gage readings on the web and the average value of two strain gage readings on the flange have been plotted with circles in these figures. Since the isoclinic and isochromatic readings were not measured at the left side of section "0", there is no photostress data shown in these figures. The theoretical values calculated from the "Vierendeel Analysis" have been plotted with a solid line in the figures for the two cases and indicate very good agreement with the strain gage data.

The normal stresses along vertical section "5" are shown in Figs. 25 and 29 for Case II and III, respectively. The strain gage data and theoretical values (Vierendeel Analysis) have been plotted in the figures, in the same manner as described above, while the photostress readings along this section are shown with the triangular points.

Along section "5", the experimental data from the photostress and strain gage readings agree reasonably well with each other and also are in good agreement with the predictions based on the Vierendeel Analysis. Thus it can be concluded

that the "Vierendeel Analysis" gives a good estimate of the normal stress distribution in the region above the web opening.

The experimentally measured normal stresses along vertical section "10" are shown in Figs. 26 and 30 for Case II and III, respectively, using the method described above, and are compared with simple beam theory ($\sigma = \frac{MY}{I}$), which is plotted as a solid line.

From these figures, it can be seen that the photostress readings agree quite well with the strain gage readings at all of the points along this section. However, the experimental data does not agree with the theoretical values calculated using simple beam theory. This difference may be explained by the fact that vertical section "10" is located in the region which is affected by the stress concentrations caused by the large web opening. This can be seen by comparing the normal stresses at the point (10,0), where the experimental values are large compressive stresses in Case II (Fig. 26). For Case III, a small tension stress occurred at the same point when the opening was enlarged to within 1/2 inch below the point shown in Fig. 30. Hence, it may be concluded that the normal stress distribution is non-linear, and simple beam theory is not suitable for determining the stresses in certain areas influenced by the stress concentration pattern. Generally speaking, these areas may cover the range from the edge of the opening to a distance about equal to the depth of the opening from the boundary of the opening.

Shear stresses along vertical section "5" are shown in Figs. 27 and 31 for Cases II and III, respectively. For both cases, the rosette strain gage readings agree quite well with the photostress readings. The theoretical values calculated from simple beam theory, $S_{xy} = \frac{VQ}{Ib}$, have been plotted in the figures. The solid lines are for shear stress calculated assuming that the total net cross section (gross section minus web opening) is effective in resisting the total shear force V = P, while the broken line is based on the assumption that the "Tee" section between the top of the opening and the top flange resists one-half of the total shear force. Comparing the theoretical values with the experimental data, it was found that the experimental data at points close to the boundary of the opening such as point (5,2) for Case II and point (5,0) for Case III, gave higher shear stresses, than the theoretical values. This may be attributed to the influence of the stress concentrations at the corners of the opening. Finally, it can be concluded that, due to the large shear stresses near the web opening, cracks could develop at the corners before the load capacity of the beam is attained.

CONCLUSIONS

From the comparison of the experimental and theoretical values obtained in this investigation, the following conclusions can be formulated:

1. Larger deflections are to be expected in a beam with a large opening in the web. Equation 2 has been demonstrated to be a good tool for determining the deflections of a beam with a large web opening.

2. For rectangular openings, the so-called "Vierendeel Method" provides a very good prediction of the normal stresses above or below the web opening.

3. The normal bending stress distribution is non-linear in a region extending from the edge of the opening a distance about equal to the depth of the beam from the opening, and simple beam theory can not be used to predict normal stresses in this region.

4. Greater shear stresses occur near the web opening than are predicted by beam theory.

5. The photostress method of experimental stress analysis and the electrical resistance strain gage techniques were found to be quite effective for determining stresses in the test beam.

6. The "Shear-difference" method was demonstrated to be an excellent method for computing the stresses at the interior points of a structure.

RECOMMENDATIONS FOR FURTHER STUDY

This study could be extended to investigate the stress distribution and deflections of a beam with different loading positions or different shapes of openings such as circles, ellipses, pentagons, hexagons, octogons, etc. Moreover, a theoretical solution for the stress distribution in the area where simple beam theory can not be applied should be developed.

Another important topic for further study is the determination of economical reinforcement requirements for beams with web openings.

ACKNOWLEDGMENTS

The author expresses his sincere appreciation to Dr. Peter B. Cooper, Associate Professor of Civil Engineering at Kansas State University, for his valuable guidance in the research and constant encouragement during the writing of this thesis. Without his efforts this research would not have been possible.

Thanks are also extended to Dr. Jack B. Blackburn, Head of the Civil Engineering Department, Dr. Robert R. Snell, and Dr. Harry D. Knostman for serving on the advisory committee.

Appreciation is also due to Mr. S. H. Hunter and Mr. W. M. Johnston for helping the author with the experimental portion of this investigation, and to Mrs. Linda Bailey for her valuable assistance in typing the manuscript of this thesis.

Table 1. Actual Dimensions

Item \ Pt.		0	1	2	3	4	5	6	7	8	9	10	11	Ave.
Top Flange	P_{in}	.494	.503	.505	.506	.505	.500	.498	.502	.504	.505	.502	.502	.502
	Q_{in}	.491	.497	.480	.483	.487	.478	.470	.472	.480	.486	.482	.474	.481
Bottom Flange	M_{in}	.485	.493	.497	.500	.496	.487	.487	.491	.491	.499	.492	.484	.491
	N_{in}	.472	.477	.487	.486	.485	.481	.471	.474	.482	.484	.487	.479	.4805
Depth	in	8.04	8.04	8.06	8.06	8.05	8.05	8.06	8.06	8.05	8.05	8.03	8.02	8.05
Flange Width	Top_{in}	7.98	7.98	8.01	8.01	8.00	7.98	7.97	8.00	8.01	8.00	8.00	8.01	8.00
	Bot_{in}	7.99	8.01	8.00	8.00	7.98	8.00	8.00	8.01	8.00	8.01	7.98	7.98	7.995

Item \ Pt.	W1	W2	W3	E1	E2	E3	Ave.
Web thickness	.327	.326	.326	.327	.324	.325	.325

Table 2. Results of Tensile Coupon Tests

	t_c in	w_c in	A_{c_2} in^2	σ_y KSI	σ_u KSI	E 10^6	δ_s % per 2in
TB1	.5030	.4930	.248	36.0	66.2	31.3	42.2%
TB2	.5035	.4835	.243	36.1	65.6	30.9	39.8%
TT1	.5000	.493	.246	35.7	65.9	31.9	38%
TT2	.5030	.486	.245	36.3	65.05	31.3	40.6%
TW1	.4985	.3270	.163	46.8	69.5	32.1	34%
TW2	.4995	.3260	.1625	51.00	70.0	28.3	31.2%

Table 3. Actual and Nominal Properties of 8W35 Beam

	DIMENSION				PHYSICAL PROPERTIES				SECTION PROPERTIES		REFERENCE LOADS	
	d	b	t_f	t_w	E	μ	σ_y	σ_u	S	Z	Py	Pu
UNITS	in.	in.	in.	in.	ksi	-	ksi	ksi	in^3	in^3	kip	kip
Nominal Values	8.12	8.027	.493	.315	29,000	.30	. .36	60	31.1	34.7	36	41.7
Actual Values	8.05	8.00	.485	.325	$\frac{31,400*}{29,600}$	.30	36.2	66.2	31.77	36.07	40	43.5

*E = 31,400 ksi for the flanges and 29,400 ksi for the web.

Table 4. Comparison of Theoretical and Experimental Deflections - Cases II and III (Elastic Range).

CASES	ITEMS	EXPTL. (in.)	Theory, Eq. 1 data (in.)	Theory, Eq. 1 Difference %	Theory, Eq. 2 data (in.)	Theory, Eq. 2 Difference %
II	Δ_{ℓ}	.1985	.1802	+ 9.1	.196	+ 1.26
	Δw	.1470	.1260	+ 14.3	.143	+ 2.5
	Δe	.1381	.1260	+ 9.5	.136	+ 1.45
III	Δ_{ℓ}	.2041	.1820	+ 11.0	.202	+ 0.9
	Δw	.147	.1260	+ 14.4	.145	+ 1.36
	Δe	.142	.1260	+ 11.7	.1425	+ 1.03

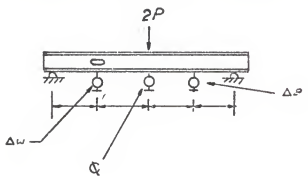

Table 5. Strain Gage Readings - Case II

Strain Gage No.	Strain gage readings in micro-inches/inch			
	4000 lbs	8000 lbs	12000 lbs	16000 lbs
1	-2	-4	-6	-8
2	+5	+9	+12	+17
3	-30	-60	-90	-120
4	-86	-169	-253	-338
5	-86	-167	-253	-337
6	-87	-169	-254	-339
7	-85	-168	-255	-342
8	-68	-131	-196	-262
9	-65	-129	-196	-262
10	-25	- 49	-74	-99
11	-43	-84	-124	-168
12	+27	+53	+78	+104
13	-18	-38	-60	-78
14	+77	+152	+228	+308
15	-27	-56	-84	-112
16	-22	-44	-66	-88
17	+52	+102	+154	+206
18	-17	-34	-52	-68

Table 6. Strain Gage Readings - Case III

Strain Gage No.	Strain gage readings in micro-inches/inch			
	4000 lbs	8000 lbs	12000 lbs	16000 lbs
1	-1	-2	-3	-4
2	+21	+41	+63	+87
3	+3	+6	+9	+13
4	-95	-192	-290	-384
5	-92	-187	-285	-380
6	-106	-214	-322	-429
7	-104	-212	-315	-431
8	-67	-133	-199	-264
9	-62	-125	-196	-265
10	-35	-71	-109	-140
11	-43	-90	-136	-176
12	+40	+80	+120	+160
13	-25	-50	-75	-100
14	+100	+200	+300	+400

Table 7. Calculation of Stresses From Strain Gages at Load 16^k - Case II.

Strain Gage at No.	Co-ordinates inches	Strain Gage Reading Micro-inches/in.	Longitudinal Stress σ_x psi
Upper Flange			
(4, 5)	(10, top)	-338	10700*
3	(10, 0)	-120	-3480
2	(10, 2)	+017	+494
1	(10, 5)	-8	-232
(6, 7)	(5, top)	-340	10762*
15	(5, 0)	-112	-3250
12	(5, 2)	+104	+3020
(8, 9)	(0, top)	-262	8270*
11	(0, 0)	-168	-4870
10	(0, 2)	-99	-2870
18	(0, 3)	-68	-1988

* Strain gage reading times E = 31,600 ksi., others times E = 29,600 ksi

Table 8. Calculation of Stresses From Strain Gages at Load 16^k - Case III

Strain Gage No. At	Co-ordinates inches	Strain Gage Reading Micro-inches/in.	Longitudinal Stress σ_x psi
(4,5)	(10, top)	-382	12000*
3	(10 0)	+13	+377
2	(10 2)	+87	+2520
1	(10, 5)	-4	-116
(6, 7)	(5, top)	-430	13600*
12	(5, 0)	+160	+4640
(8, 9)	(0, top)	-265	8400*
(11)	(0, 0)	-176	-5100
(10)	(0, 1)	-142	-4060

*Strain gage reading times E = 31,600 ksi., others times E = 29,600 ksi.

Table 9. Isoclinic Angles and Isochromatic Reading - Case II

Point	Loads	ISOCHROMATIC READING 16000 lbs	12000 lbs	8000 lbs	4000 lbs	ISOCLINIC
0	1	.240	.170	.120	.060	63.0
0	2	.120	.08	.050	.025	28.0
2	0	.390	.290	.195	.095	55.0
2	1	.245	.185	.120	.060	49.0
2	2	.08	.060	.040	.020	16.0
4	0	.380	.290	.190	.095	56.0
4	1	.395	.300	.200	.100	50.0
4	2	.270	.200	.130	.065	35.0
5	0	.280	.210	.193	.070	52.0
5	1	.320	.240	.160	.080	50.0
5	2	.410	.300	.210	.106	36.0
6	0	.186	.140	.095	.050	73.0
6	1	.280	.170	.140	.070	62.0
6	2	.300	.225	.150	.075	53.0
6	3	.440	.325	.215	.125	0.00
6	4	.49	.37	.25	.125	0.00
6	5	.330	.250	.170	.080	0.00
8	0	.220	.170	.110	.050	80.0
8	1	.220	.170	.120	.060	45.0
8	2	.190	.140	.100	.050	21.0
8	3	.330	.400	.260	.130	27.0
8	4	.600	.450	.300	.150	36.0
8	5	.675	.500	.340	.170	47.0
10	0	.310	.250	.150	.075	60.0
10	1	.190	.140	.095	.050	44.0
10	2	.310	.230	.150	.090	38.0
10	3	.360	.290	.190	.095	36.0
10	4	.475	.315	.235	.120	38.0
10	5	.490	.360	.250	.125	47.0
12	0	.250	.290	.130	.065	61.0
12	1	.240	.180	.120	.060	44.0
12	2	.300	.230	.150	.075	32.0
12	3	.305	.225	.155	.080	36.0
12	4	.430	.320	.210	.110	38.0
12	5	.460	.350	.230	.120	43.0

Table 10. Isoclinic Angles and Isochromatic Readings - Case III.

Point	Loads	ISOCHROMATIC READING 16000 lbs	12000 lbs	8000 lbs	4000 lbs	ISOCLINIC degree
2	0	.29	.22	.15	.07	20.0
2	1	.30	.23	.15	.06	0.0
4	0	.40	.32	.22	.12	26.0
4	1	.80	.60	.40	.20	0.0
5	0	.41	.30	.20	.10	30.0
5	1	1.85	1.40	.95	.48	0.0
6	0	.16	.12	.08	.04	0.0
6	1	.90	.70	.45	.25	40.0
6	2	1.10	.81	.53	.28	40.0
6	3	.30	.20	.15	.10	0.0
6	4	.20	.15	.10	.05	0.0
6	5	.20	.15	.09	.05	0.0
6	6	.19	.14	.08	.04	0.0
8	0	.20	.15	.09	.05	10.0
8	1	.39	.29	.20	.10	12.0
8	2	.24	.18	.12	.06	26.0
8	3	.27	.20	.14	.07	42.0
8	4	.21	.15	.11	.06	43.0
8	5	.16	.12	.08	.04	51.0
8	6	.16	.12	.08	.04	53.0
10	0	.19	.14	.09	.05	10.0
10	1	.24	.18	.12	.06	16.0
10	2	.25	.19	.13	.06	23.0
10	3	.32	.24	.16	.08	42.0
10	4	.30	.22	.15	.07	44.0
10	5	.31	.23	.15	.08	44.0
10	6	.26	.20	.13	.07	50.0
12	0	.12	.09	.06	.03	30.0
12	1	.22	.17	.12	.06	32.0
12	2	.20	.15	.10	.05	33.0
12	3	.28	.21	.14	.07	36.0
12	4	.26	.19	.13	.07	40.0
12	5	.26	.19	.13	.07	45.0
12	6	.14	.11	.07	.04	50.0

Table 11. Normal Stress Calculation Along Vertical Section 5 at Load 12 kips - Case II.

IJ	$\Delta Sxy \frac{\Delta x}{\Delta y}$	σy	$\sigma_1 - \sigma_2$	Sxy	$\sqrt{(\sigma_1-\sigma_2)^2-4Sxy^2}$	$\sigma x = \sigma y \pm \sqrt{(\sigma_1-\sigma_2)^2-4Sxy^2}$
53	-1800	0	3600	0	3600	+3600
52	-1335	+1335	11350	5396	630	+2005
51	+950	+425	8864	4429	326	+99
50	+1400	-975	7706	3737	1852	-2827

Table 12. Normal Stress Calculation Along Vertical Section 10 - Case II

(1) I	J	(2) $\Delta Sxy \frac{\Delta y}{\Delta x}$	(3) σ_x	(4) $\sigma_1 - \sigma_2$	(5) Sxy	(6) $(\sigma_1-\sigma_2)^2$	(7) $4Sxy^2$	(8) $\sqrt{(6)-(7)}$	(9) $\sigma y = (3) \pm (8)$
6	4		0	13573	0	1842264000	0	13573	-13573
8	4	1400	-1400	16620	7897	276224360	249494330	5170	-6500
10	4	-2000	600	13150	6380	173119900	162817640	3210	-2610
12	4	-2200	+2800	11911	5775	141872020	133429170	2906	-109

(1)		(2)	σy(3)	(4)	(5)	(6)	(7)	(8)	σx(9)
10	5		-2110	13573	6770	184226400	183373630	923	-1087
10	4	500	-2610	13150	6380	173119900	162817640	3210	+600
10	3	312	-2910	10027	4764	100548820	90818660	3119	+209
10	2	+50	-2960	8587	3713	73736537	55148512	4311	+1351
10	1	-50	-3010	6371	2900	40589663	39337718	1119	-1891
10	0	-100	-3110	6648	3310	44195918	43113012	1020	-4020

Table 13. Normal Stress Calculation Along Horizontal Section 5 - Case III

(1) I	J	(2) $\Delta Sxy\frac{\Delta x}{\Delta y}$	(3) σx	(4) $\sigma_1 - \sigma_2$	(5) Sxy	(6) $(\sigma_1-\sigma_2)^2$	(7) $4Sxy^2$	(8) $\sqrt{(6)-(7)}$	(9) $\sigma y = \sigma x \pm (8)$
6	5		0	5540	0	30691582	0	5540	-5540
8	5	50	-50	4432	2168	19642614	18805997	1001	+951
10	5	400	-450	285	4291	73736537	73655572	285	-735
12	5	840	-1209	7202	3601	51868798	51868660	12	-1221

Calculation of Normal Stress Along Vertical Section 10 in Case IV.

(1) I	J	(2) $\Delta Sxy\frac{\Delta y}{\Delta x}$	(3) σy	(4) $(\sigma_1-\sigma_2)$	(5) Sxy	(6) $(\sigma_1-\sigma_2)^2$	(7) $4Sxy^2$	(8) $\sqrt{(6)-(7)}$	(9) $\sigma x = \sigma y \pm (8)$
10	5	250	-735	8587	4291	73736537	73655572	285	-450
10	4	259	-994	8310.0	4152	69055045	68980288	725	-289
10	3	75	-1069	8864	3978	78570509	6333716	3300	+2200
10	2	85	-1154	6648	2540	44195918	2584637	4287	+3133
10	1	100	-1144	6468	1753	44175722	12293083	5101	+3956
10	0	125	-1369	4563	1321	20713203	11753270	3048	+1618

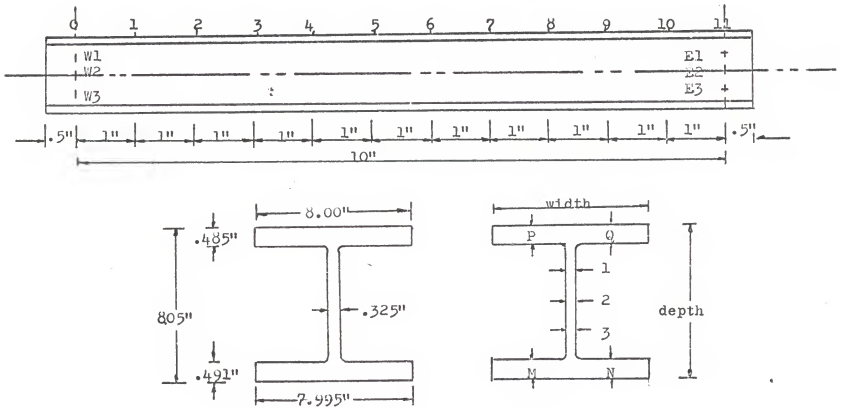

Fig. 1 Locations For Measuring Actual Dimensions

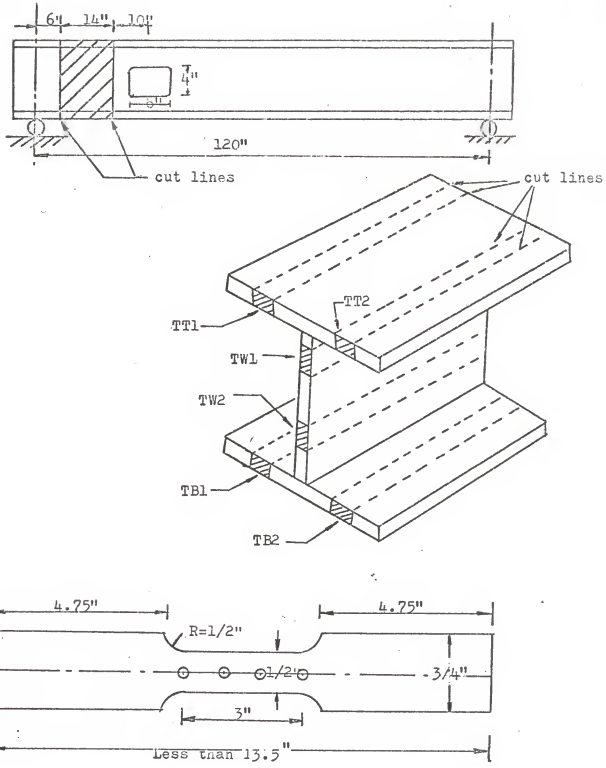

Fig. 2 Tensile Coupon Specimens

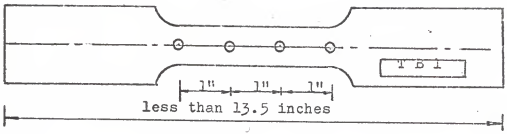

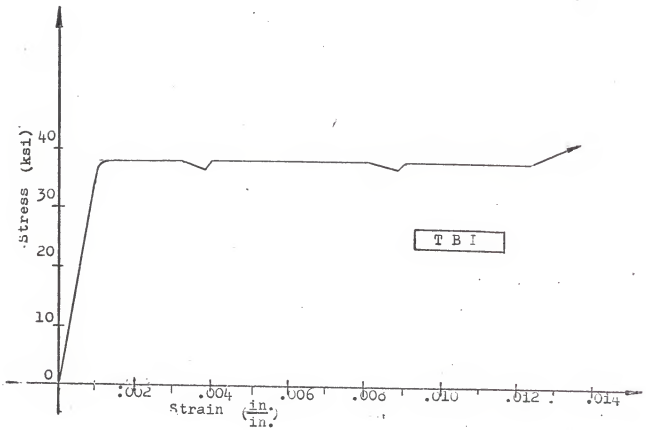

Fig. 3 Typical Coupon Stress-Strain Curve

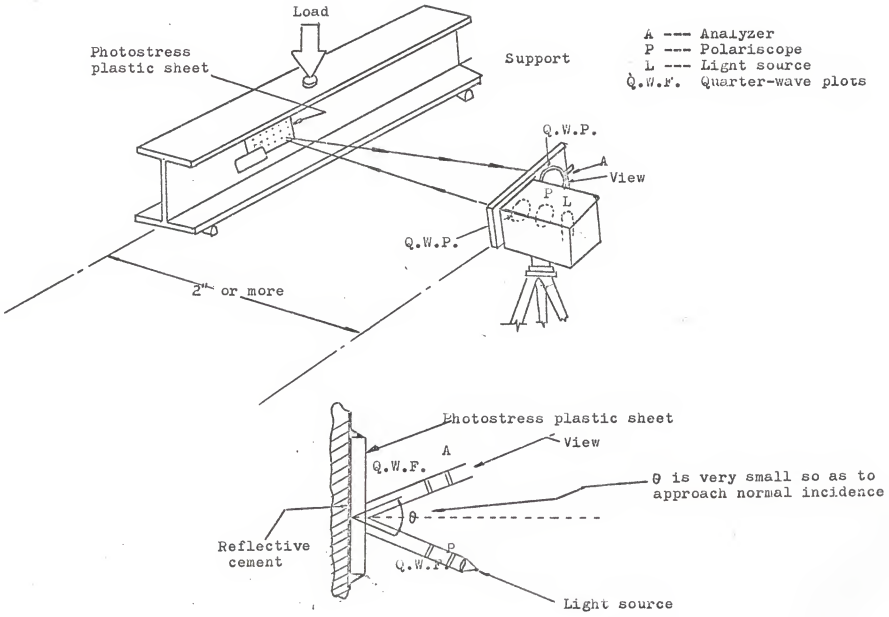

Fig. 4 Photostress Measurements

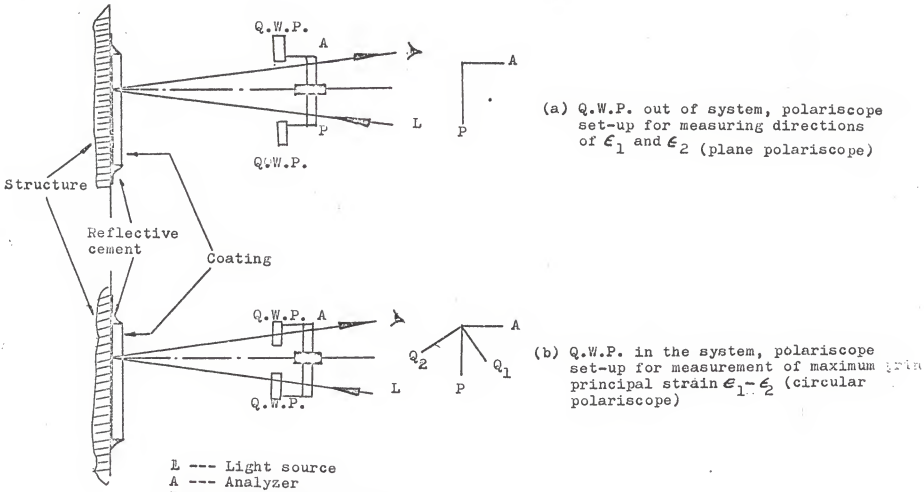

(a) Q.W.P. out of system, polariscope set-up for measuring directions of ϵ_1 and ϵ_2 (plane polariscope)

(b) Q.W.P. in the system, polariscope set-up for measurement of maximum principal strain $\epsilon_1 - \epsilon_2$ (circular polariscope)

Fig. 5 Optical System For Photostress Measurements

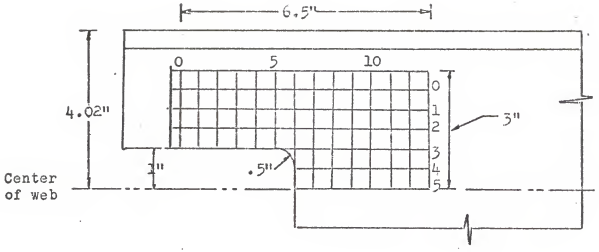

(a) Case II

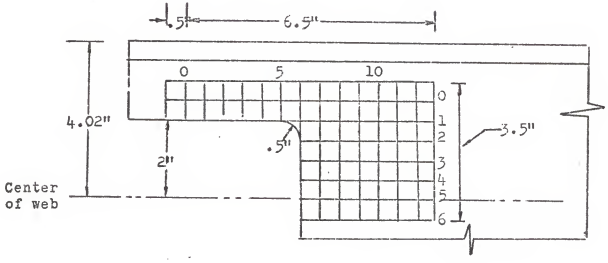

(b) Case III

Fig. 6 Locations Of Photostress Sheets

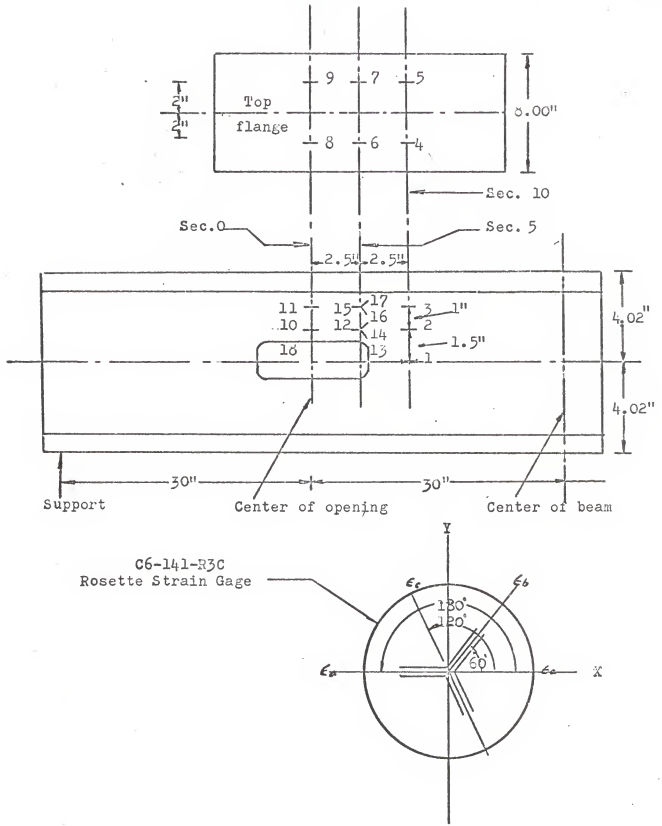

Fig. 7 Arrangement of Strain Gages For Case II

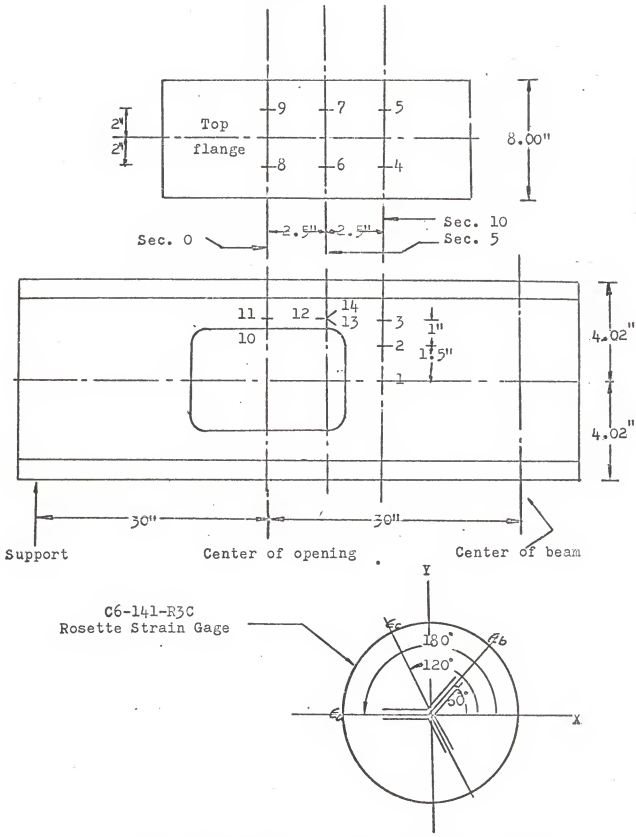

Fig. 8 Arrangement of Strain Gages For Case III

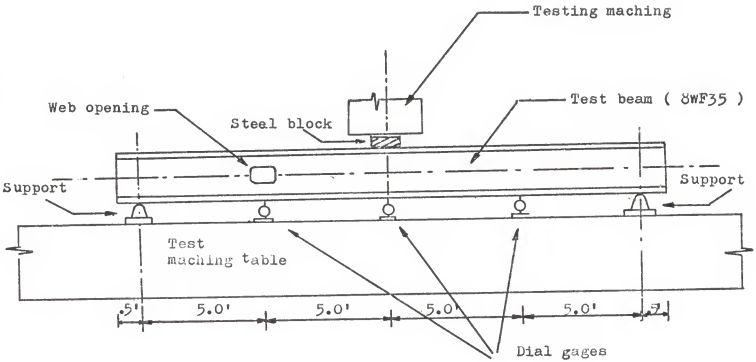

Fig. 9 General Setup Of The Experiment

Fig. 10 Photograph of the General Set-up of the Experiment

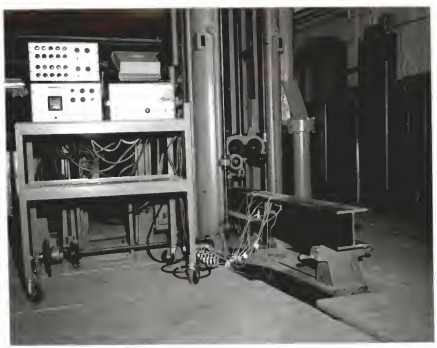

Fig. 11 Photograph of The Beam With Digital Strain Indicator

(Budd Model A110 C-1ot And C-10 Ltc)

Fig. 12 Photograph of The Beam with Large Field Meter And Its Accessories

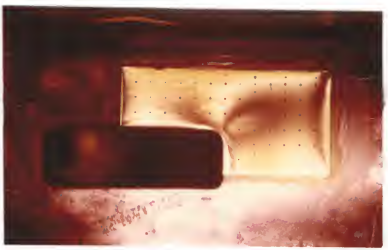

(a) Case II-(30)

(b) CaseIII-(45)

Fig.13 Photograph of Isoclinics - Case II and Case III

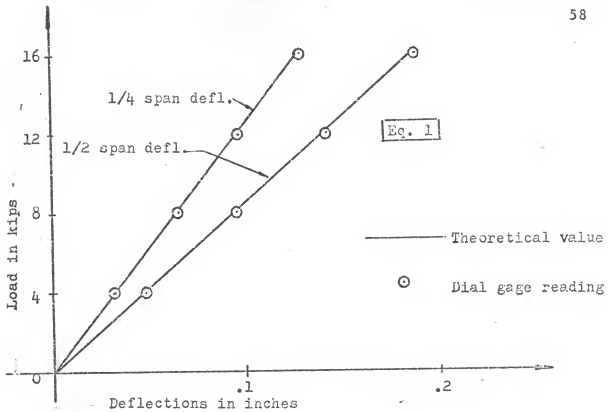

Fig. 14 Deflections Of Beam-Case I

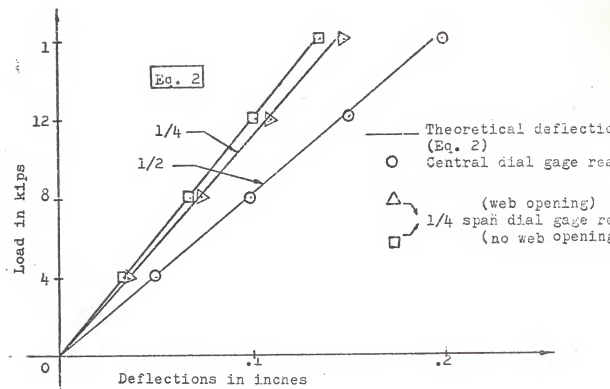

Fig. 15 Deflections Of Beam-Case II

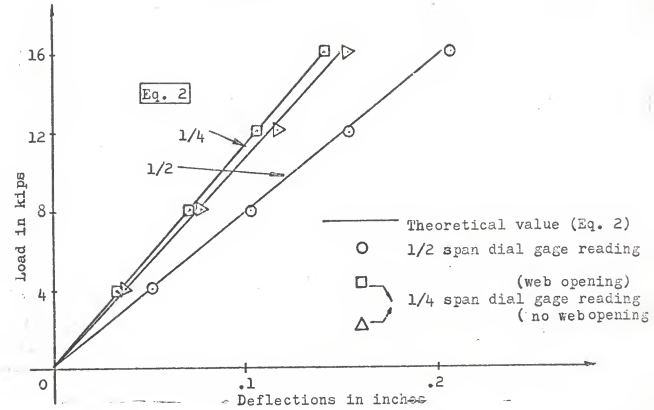

Fig. 16 Deflections Of Beam-Case III

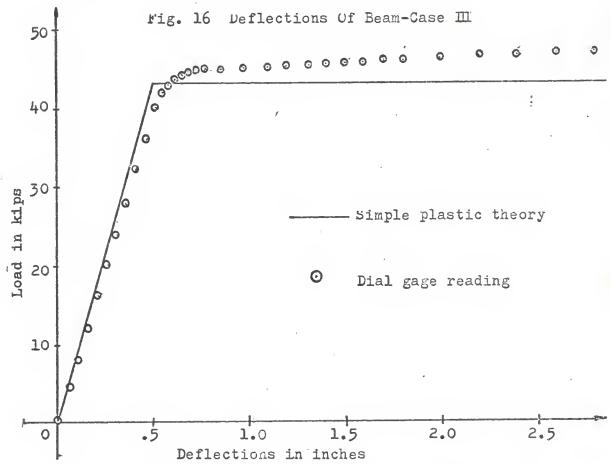

Fig. 17 Deflections of Beam-Case IV

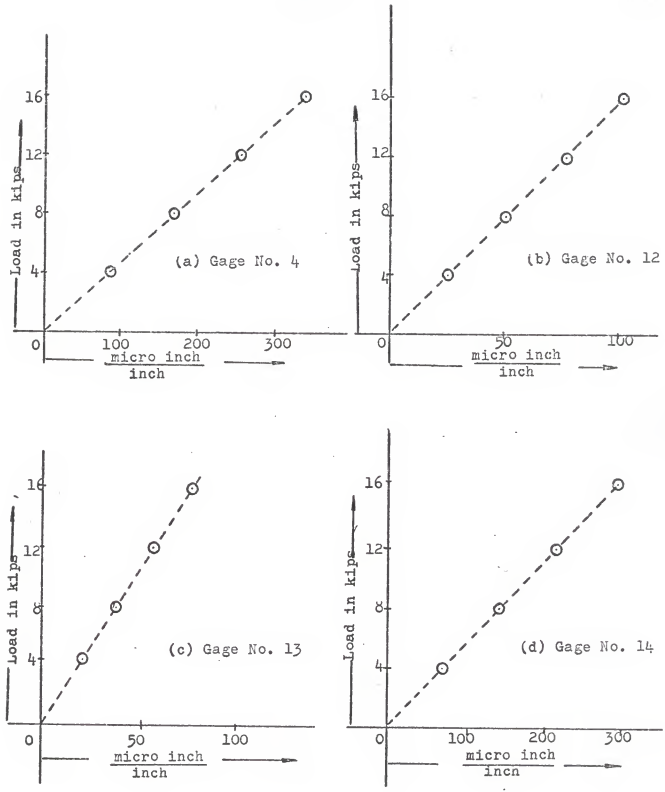

Fig. 18 Typical Load-Strain Plots-Case II

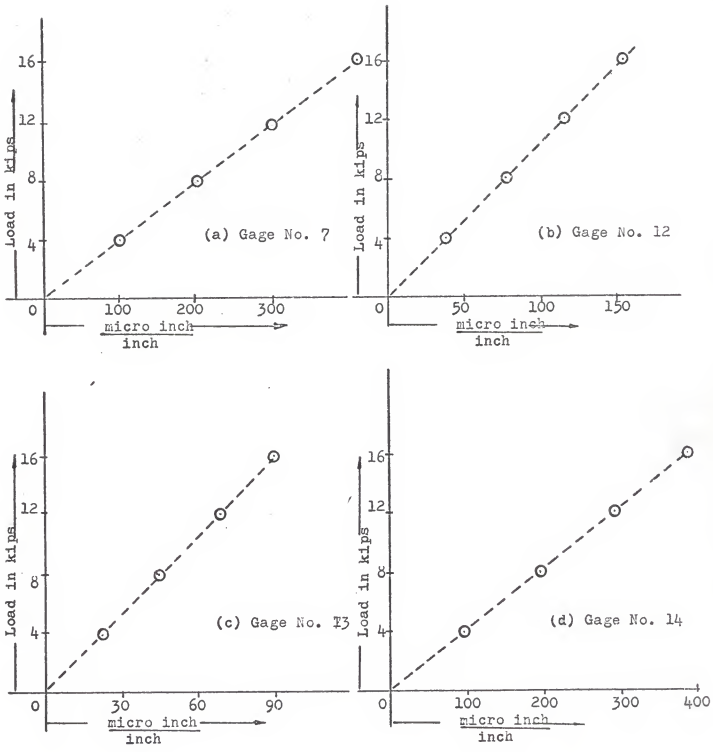

Fig. 19 Typical Load-Strain Plots-Case III

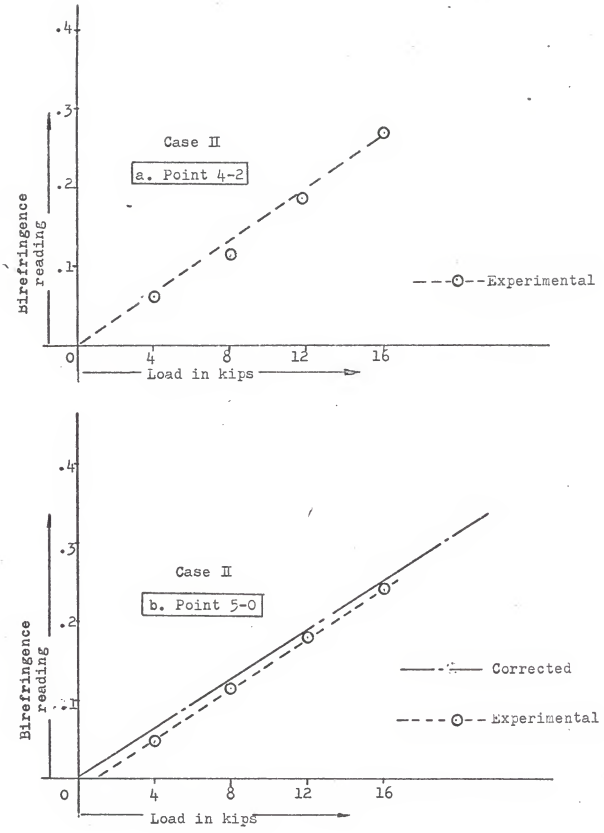

Fig. 20a Correction for Residual Birefringence

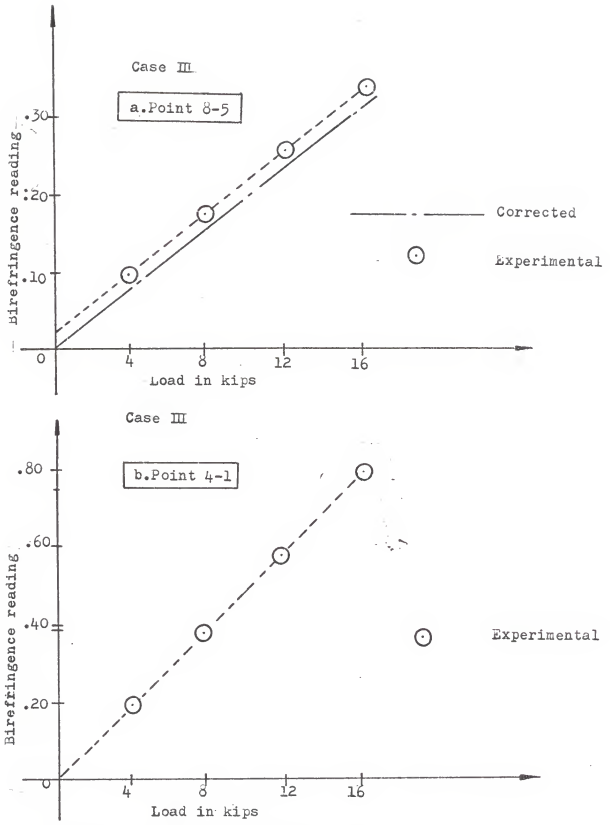

Fig. 20b Correction For Residual Birefringence

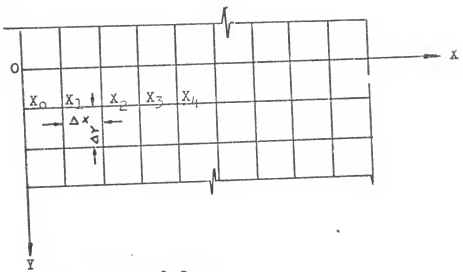

a. General Case

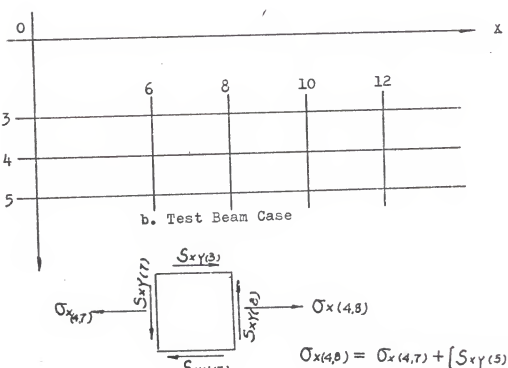

b. Test Beam Case

Fig. 21 Coordinate System For Shear-difference Method

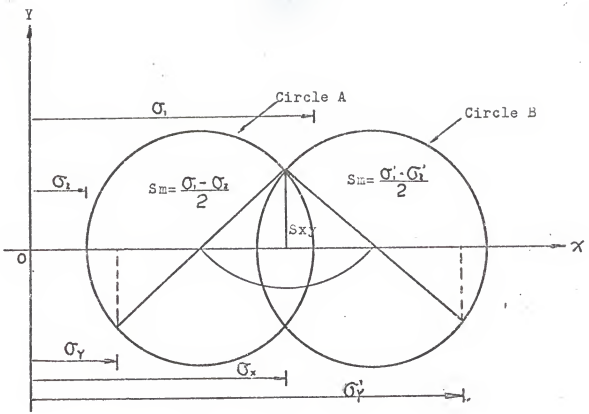

Fig. 22 Two Possible Constructions Of Mohr's Circle For The Same Given $(\sigma_1 - \sigma_2)$, σ_x, σ_Y

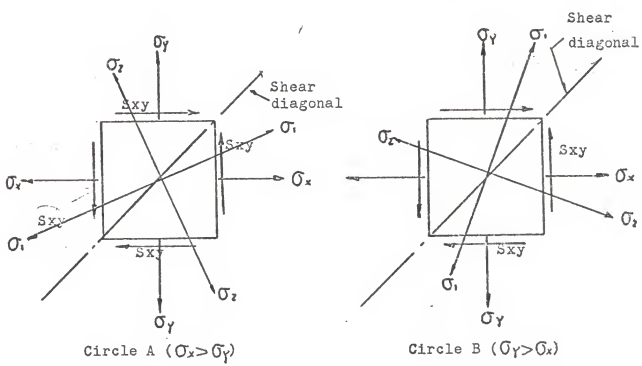

Fig. 23 Relative Magnitudes Of σ_1 And σ_Y

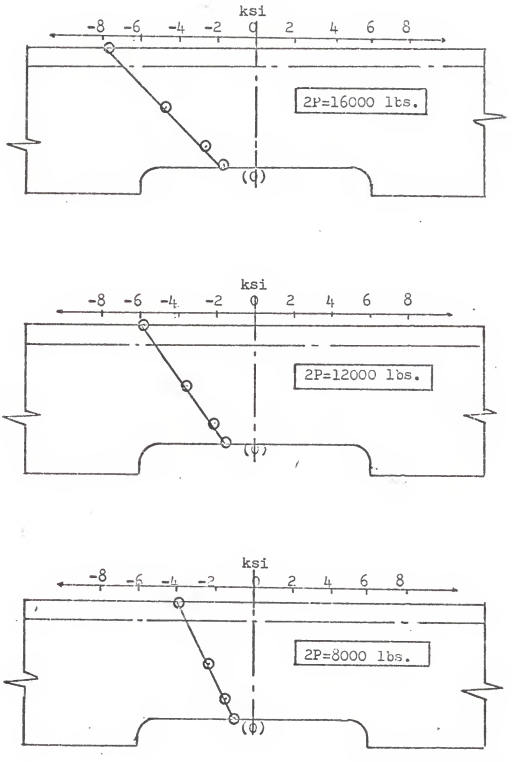

Fig. 24 Normal Bending Stresses Along Vertical Section "C"-Case II

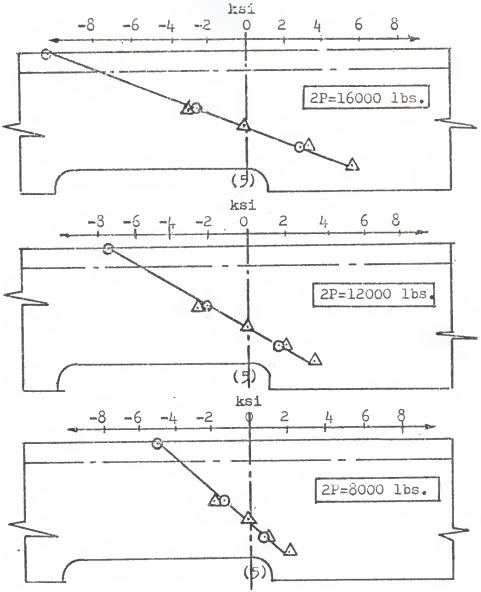

Fig. 25 Bending Stresses Along Vertical Section "5"-Case II

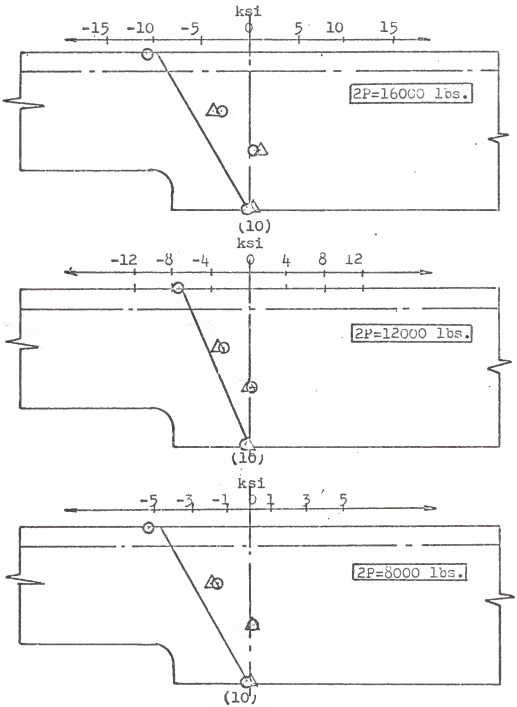

Fig. 26 Bending Stresses Along Vertical Section "10"-Case II

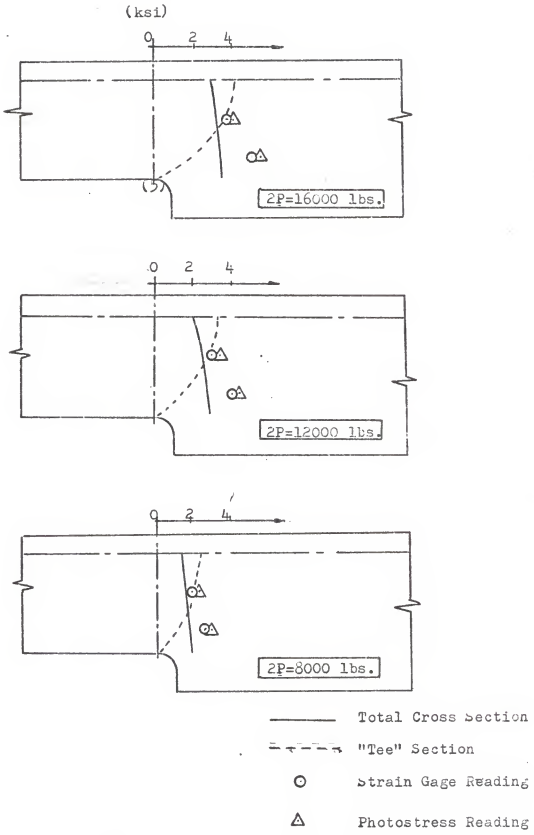

Fig. 27 Shear Stresses Along Vertical Section "5"-Case II

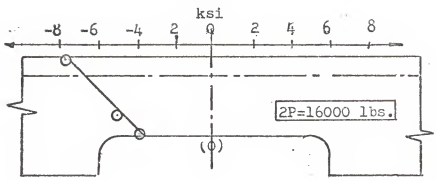

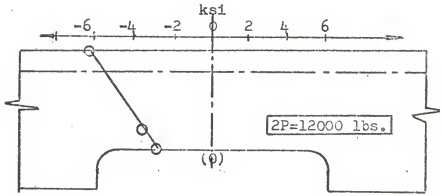

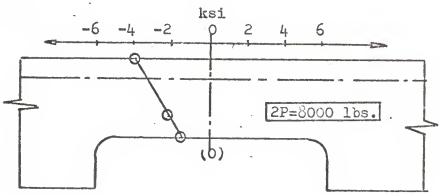

——— Vierendeel Analysis

⊙ Strain gage reading

Fig. 28 Bending Stresses Along Vertical Section "O"-Case III

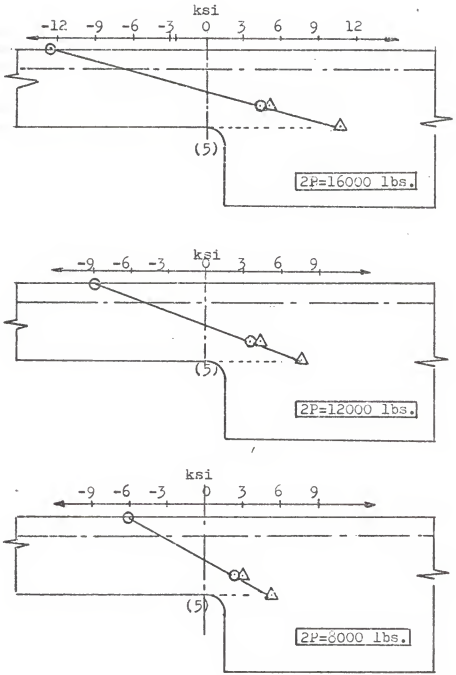

Fig. 29 Bending Stresses Along Vertical Section "5"-Case III

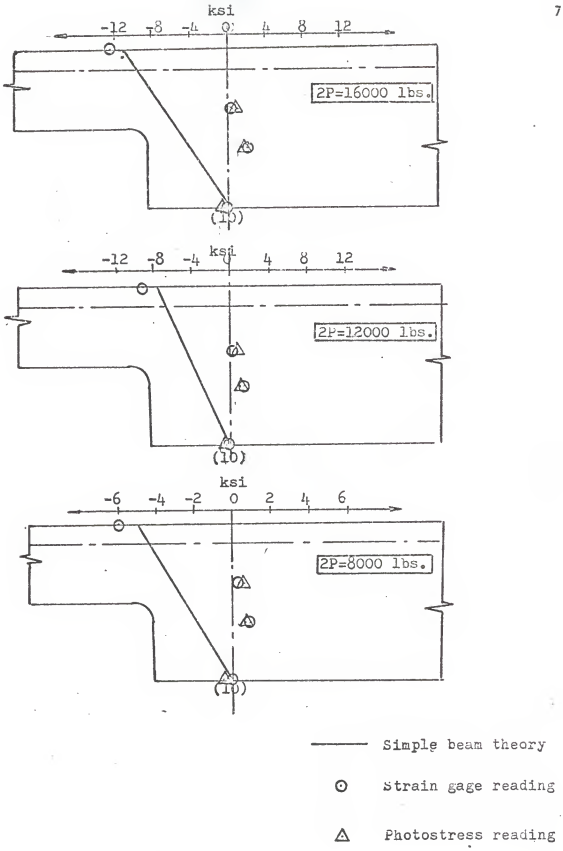

Fig. 30 Bending Stresses Along Vertical Section "10"-(Case III)

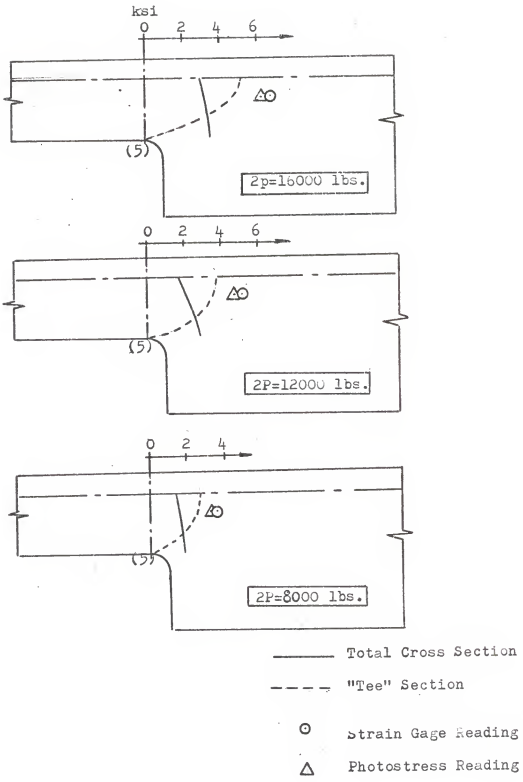

Fig. 31 Shear Stresses Along Vertical Section "5"- Case II

NOTATION

A	area of gross beam
A_c	cross section of coupon test specimen
A_o	area of section through web opening
a	half length of rectangular opening
b	width of beam
C	birefringence reinforcing factor
d	depth of beam
E	Modulus of Elasticity
f	fringe value
G	modulus of rigidity
h	half depth of rectangular opening
I	moment of inertia of gross beam
I_o	moment of inertia of section through opening
I_t	moment of inertia of tee-section
K	strain optical sensitivity constant of photostress coating
k	shear sharp factor
M	moment due to applying load
m	moment due to virtual load
N_n	fringe order
P	applied load
P_y	yield load
P_u	ultimate load
r	corner radius of opening
S	section modulus
S_{xy}	shear stress

t_c	thickness of coupon test specimen
t_f	thickness of beam flange
t_p	thickness of photostress coating
t_w	thickness of beam web
V	shear force due to applied load
v	shear force due to virtual load
w_c	width of coupon test specimen
x, y	coordinate system
Y	transverse distance from centroid of beam
$\overline{Y}$	distance from boundary of opening to centroid of tee-section
Y_t	distance from center of opening
Z	plastic modulus
σ_x	normal stress in x-direction
σ_y	normal stress in y-direction
$(\sigma_1-\sigma_2)$	principle stress difference
δ	elongation of coupon test specimen in two inches
δ_n	relative retardation
Δ	deflection of beam
ε	strain gage reading
$(\varepsilon_1-\varepsilon_2)$	principle strain difference
λ	wave length of light
θ	isoclinic angle

REFERENCES

1. Muskhelishvili, N. I., Some Basic Problems of the Mathematical Theory of Elasticity, 2nd Edition, P. Noorhoff, Ltd., Croningen, The Netherlands, 1963.

2. Heller, Brock and Bart, "The stresses Around Rectangular Openings with Rounded Corners in a Beam Subjected to Bending with Shear," Proc., 4th National Congress of Applied Mechanics, 1962.

3. Bower, J. E., "Elastic Stresses Around Holes in Wide-Flange Beams," Journal of the Structural Division, ASCE, Vol. 92, No. ST2, April, 1966.

4. Bower, J. E., "Experimental Stresses in Wide Flange Beams with Holes," Journal of Structural Division, ASCE, Vol. 92, No. ST5, Oct., 1966.

5. Redwood, R. G., and J. O. McCutcheon, "Wide-Flange Beams Containing Large Unreinforced Web Openings," Structure Mechanics Series, No. 2, McGill University, Montreal, Canada, Sept., 1967.

6. Segner, Edmund, P., "Reinforcement Requirements for Girder Web Openings," Journal of the Structural Division, ASCE, Vol. 90, No. ST3, June, 1964.

7. Cato, S. L., "Web Buckling Failure of Built-up Girder with Rectangular Holes," M.S. thesis, Oregon State University, June, 1964.

8. Arora, J., "Experimental Stress Analysis of an I-Beam with a Rectangular Web Cutout," M.S. thesis, Kansas State University, 1967.

9. Hendry, A. W., "The Stress Distribution of a Simply Supported Beam of I-Section Carrying A Central Load," Proc., Society for Exp. Stresses Analysis, VII, No. 2, 1950.

10. American Institute of Steel Construction. Steel Construction Manual, 6th Edition, New York, 1963.

11. ASTM Standards for Physical and Mechanical Testing of Material. Part 31, May, 1967.

12. Michalos, James, Structural Mechanics and Analysis, The MacMillan Co., New York, 1965.

13. Beedle, Lynn S., Plastic Design of Steel Structures, John Wiley & Sons, 1961.

14. Singer, Ferdinand L., Strength of Materials, Second Edition, Happer & Publishers, 1962.

15. Budd Company"Instrument Division," Phoenixville, Pennsylvania.

    (a) Instruction Manual for Photostress LF/M and its Accessories

    (b) Instruction Manual for Digital Strain Indicator (Model A-110).

16. Dove, Richard C., Paul H. Adams, Experimental Stress Analysis and Motion Measurement, Charles E. Morril Books, Inc., Columbus, Ohio, 1964.

17. Holister, G. S., Experimental Stress Analysis, Cambridge University Press, Cambridge, England, 1967.

18. Roark, R. J., "Formulas for Stress and Strain," Third Edition, McGraw-Hill Book Co., New York, 1954.

Appendix A, Flow Diagram for Computer Program

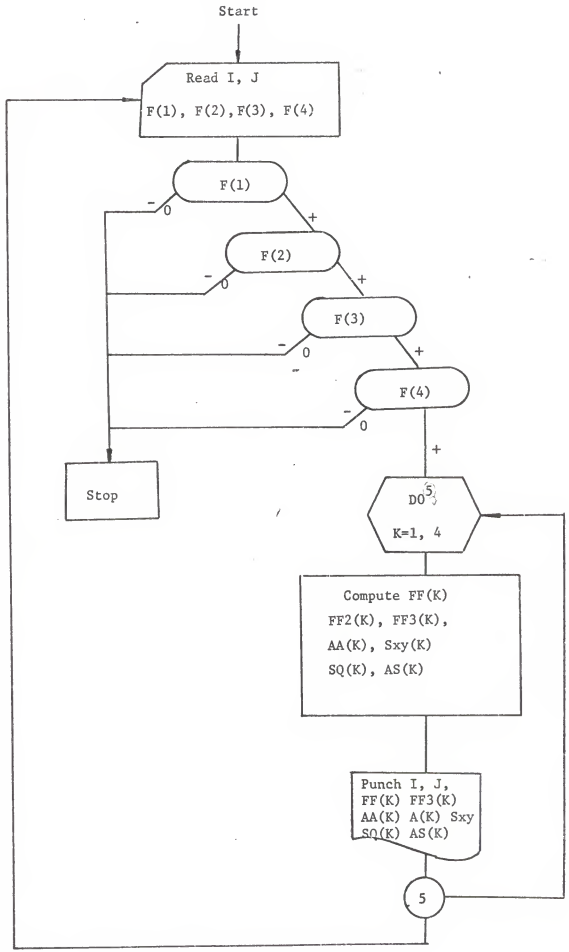

Table A-1. Sample Input Data for Computer Program

A Sample of Input Data for the Computer Program No. 2 - Case III

I	J	F(1)	F(2)	F(3)	F(4)	A
8	0	.20	.15	.09	.05	10.0
8	1	.39	.29	.20	.10	12.0
8	2	.24	.18	.12	.06	26.0
8	3	.27	.20	.14	.07	42.0
8	4	.21	.15	.11	.06	43.0
8	5	.16	.12	.08	.04	51.0

Table A-2. Output of Computer Program

J	I	$\sigma_1-\sigma_2$	$(\sigma_1-\sigma_2)^2$	$4Sxy^2$	Sxy	SinZθ	θ	F(K)	$\sqrt{(\sigma_1-\sigma_2)^2-4Sxy^2}$
5	10	8587.0	73736537.0	73655572.0	4291.1	.99945	44.0	.310	285.
5	10	6371.0	40589663.0	40545052.0	3183.8	.99945	44.0	.230	211.
5	10	4155.0	17264017.0	17245078.0	2076.4	.99945	44.0	.150	138.
5	10	2216.0	4910655.5	4905263.2	1107.4	.99945	44.0	.080	73.
4	10	8310.0	69056045.0	68980288.0	4152.7	.99945	44.0	.300	275.
4	10	6094.0	37136838.0	37096061.0	3045.3	.99945	44.0	.220	202.
4	10	4155.0	17264017.0	17245078.0	2067.4	.99945	44.0	.150	138.
4	10	1939.0	3759723.5	3755595.2	969.0	.99945	44.0	.070	64.
3	10	8864.0	78570509.0	63327316.0	3978.9	.89777	42.0	.320	3300.
3	10	6648.0	44195918.0	35621621.0	2984.2	.89777	42.0	.240	2928.
3	10	4432.0	19642614.0	15831835.0	1989.5	.89777	42.0	.160	1952.
3	10	2216.0	4910655.5	3957956.2	994.7	.89777	42.0	.080	976.
2	10	6648.0	44195918.0	25821637.0	2540.8	.76437	23.0	.240	4287.
2	10	4986.0	24860182.0	14524688.0	1905.6	.76437	23.0	.180	3215.
2	10	3324.0	11048972.0	6455418.0	1270.4	.76437	23.0	.120	2143.
2	10	1662.0	2762244.1	1613855.1	635.2	.76437	23.0	.060	1072.
1	10	6648.0	44195918.0	12293083.0	1753.1	.52740	16.0	.240	5101.
1	10	4986.0	24860182.0	6914860.4	1314.8	.52740	16.0	.180	4236.
1	10	3324.0	1104897s.0	3073268.9	876.5	.52740	16.0	.120	2824.
1	10	1662.0	2762244.1	768317.5	438.3	.52740	16.0	.060	1412.
0	10	5263.0	27699142.0	3183256.7	892.1	.33900	10.0	.190	3048.
0	10	3878.0	15038888.0	1728306.1	657.3	.33900	10.0	.140	2251.
0	10	2493.0	6215047.8	714248.6	422.6	.33900	10.0	.090	1523.
0	10	1385.0	1918225.2	220447.2	234.8	.33900	10.0	.050	741.

Notation for the Computer Program

I, J	Coordinate system of photostress calculation (see Fig. 4)
F(1)	isochromatic reading at load 16 kips
F(2)	isochromatic reading at load 12 kips
F(3)	isochromatic reading at load 8 kips
F(4)	isochromatic reading at load 4 kips
FF2	principal stress differences $(\sigma_1-\sigma_2)$
FF3	$(\sigma_1-\sigma_2)^2$
A	isoclinic angles i0
AA	Sin 20
S_{xy}	shear stresses
SQ	Four times the square of shear stress = $4(S_{xy})^2$
AS	$\sqrt{(\sigma_1-\sigma_2)^2 - 4S_{xy}^2}$

APPENDIX B. VIERENDEEL METHOD OF ANALYSIS

1. Introduction

The well-known "Vierendeel Method" for the analysis of a beam with a web opening is based on an early presentation by Roark[18]. Application of this method to steel beams with web openings is generally referred to as the approximate "Vierendeel Analysis".

In past few years, the method has been studied by several researchers and has been outlined by Bower.[4] However, it actually needs little more than a brief introduction since the method is very straight-forward.

2. Assumptions

The assumptions of the Vierendeel Method can be divided into two parts.

a. Consider a beam in bending with a web opening as shown in Fig. B1. If the web opening is centered on the neutral axis of the beam, it is assumed that the shear at the opening is equally divided between the upper and lower tee-sections ($V = P$, $\frac{V}{2} = 0.5P$)

b. It is assumed that a point of contraflexure occurs at the center of the opening span, considering "shear-bending" only.

3. Analysis

The stresses around the hole are obtained simply by a summation of two effects at the hole. First, the gross-beam bending moment stresses are calculated as for a solid beam. The moment in Fig. B1 is given by $M = P(U+X)$ and the bending stresses by $\sigma_{x1} = \frac{MY}{I}$. (B-1)

The second, the tee-section "shear bending" moment stresses are calculated as for a cantilever using the previously described assumptions. The stresses caused by $\frac{V}{2} = 0.5P$ are computed by simple beam theory applied to the tee-section above and below the opening. Thus, the shear force causes shear stresses S_{xy} in the stem and bending stresses σ_{x2} given by

$$S_{xy} = \frac{V}{2I_t}(\bar{Y}^2 - Y_t^2) = \frac{P}{2I_t}(\bar{Y}^2 - Y_t^2) \tag{B-2}$$

$$\sigma_{x2} = \frac{VXY_t}{2I_t} = \frac{PXY_t}{2I_t} \tag{B-3}$$

So the resulting equation for total normal bending stress is

$$\sigma_x = -\frac{MY}{I} \pm \frac{PXY_t}{2I_t} \tag{B-4}$$

where I_t = the moment of inertia of one Tee-section about its centroid, $\bar{Y}$ = the distance from the boundary of the opening to the centroid of tee-section, Y_t = distance from the neutral

axis of the tee-section (Y_t is positive for points between the hole and the neutral axis of the tee-section), I = the moment of inertia of the net beam about its centroidal axis and Y = transverse distance from the centroid.

4. Calculations for This Investigation

Fig. B02 shows the dimensions of the tee-sections used in the Vierendeel Analysis of Cases II and III. The system of coordinates for the calculations is shown in Figs. B3 and B4. The calculations of the normal bending stresses σ_x, along vertical sections "0" and "5", which are based on Eqs. B1 and B3 are summarized in Tables B1 and B2. The total normal stresses for Cases II and III are given in Table B3 and were obtained by summing the values in Tables B1 and B2. Table B4 shows numerical values of the total normal stresses for Cases II and III. These total bending stresses are also presented graphically for the two cases for a load of 16 kips in Fig. B5. Some other plots of the stresses resulting from the Vierendeel Analysis are shown in Figs. 24, 25, 28 and 29, and are compared with the experimental values elsewhere in this thesis.

Table B-1. Theoretical Bending Stresses Determined by the Vierendeel Method - Gross Beam

(a) Case II

Point	M	Y	I_n	$\frac{MY}{I_n}$
A_1	32.5P	1.00	120.4	-.265P
B_1	"	1.50	"	-.398P
C_1	"	2.50	"	-.664P
D_1	"	4.03	"	-1.070P
E_1	30.0P	1.00	"	-.242P
H_1	"	4.03	"	-.975P

(b) Case III

Point	M	Y	I_n	$\frac{MY}{I_n}$
A_2	32.5P	2.000	124.6	-.517P
B_2	32.5P	2.625	"	-.680P
C_2	32.5P	3.125	"	-.807P
D_2	32.5P	4.030	"	-.104P
E_2	30.5P	2.000	"	-.477P
H_2	30.0P	4.030	"	-.960P

Table B-2. Theoretical Bending Stresses Determined by the Vierendeel Method - Tee Section

(a) Case II.

Point	V	X	Y_t	VXY_t	I_t	$VXY_t/2I_t$
A_1	P	2.5	2.56	6.4	3.14	1.01
B_1	"	"	2.06	5.15	"	0.82
C_1	"	"	1.00	2.65	"	0.42
D_1	"	"	-.49	1.23	"	0.195
E_1	"	"	2.56	0.00	"	0.00
F_1	"	"	2.06	0.00	"	0.00
G_1	"	"	1.06	0.00	"	0.00
H	"	"	-.49	0.00	"	0.00

(b) Case III.

Point	V	X	Y_t	VXY_t	I_t	$VXY_t/2I_t$
A_2	P	2.5	1.63	4.06	1.47	+2.70
B_2	"	"	0.995	2.49	"	1.53
C_2	"	"	0.495	1.24	"	0.81
D_2	"	"	-.43	1.07	"	-.705
E_2	"	0	1.63	0.00	"	0.00
H_2	"	0	-.43	0.00	"	0.00

Table B-3. Total Theoretical Bending Stresses Determined by the Vierendeel Method.

(a) Case II

Point	$\frac{MY}{I_n}$	$\frac{VXY_t}{2I_t}$	$\frac{MY}{2I_n} + \frac{VXY_t}{2I_t}$
A_1	-.265P	+1.00P	0.73P
B_1	-.398P	+0.82P	0.42P
C_1	-.664P	+0.421P	-.22P
D_1	-1.070P	-0.195P	-1.265P
E_1	-.242P	0.000	-0.242P
H_1	-.975P	0.000	-0.975P

(b) Case III

Point	$\frac{MY}{I_n}$	$\frac{VXY_t}{2I_t}$	$\frac{MY}{2I_n} + \frac{VXY_t}{2I_t}$
A_2	-.517P	+2.670P	2.150P
B_2	-.680P	+1.530P	0.850P
C_2	-.807P	+0.810P	0.003P
D_2	-1.040P	-0.705P	-1.700P
E_1	-.477P	0.00	-0.477P
H_1	-.960P	0.00	-0.960P

Table B-4. Theoretical Stress Calculation Using the Virendeel Method.

(a) Case II

Point	σ_x	2P=16000	2P=12000	2P=8000	2P=4000
A_1	0.730P	+95800	+4360	+2900	+1450
B_1	0.420P	±3360	+2520	+1680	+840
C_1	-0.220P	-1760	-1320	-880	-440
D_1	-1.265P	-10100	-7550	-5050	2525
E_1	-0.242P	-1930	-1450	-965	-483
H_1	-0.975P	-7800	-5800	-3900	-1950

(b) Case III

Point	σ_x	2P=16000	2P=12000	2P=8000	2P=4000
A_2	+2.150P	17200	12900	8620	4310
B_2	+0.850P	+6780	+5100	+3400	+1700
C_2	+0.003P	+24	+18	+12	+6
D_2	-1.700P	-13600	-10200	-6800	-3400
E_2	-0.477P	-3820	-2860	-1910	-955
H_2	-0.960P	-9660	-5775	-4830	-2415

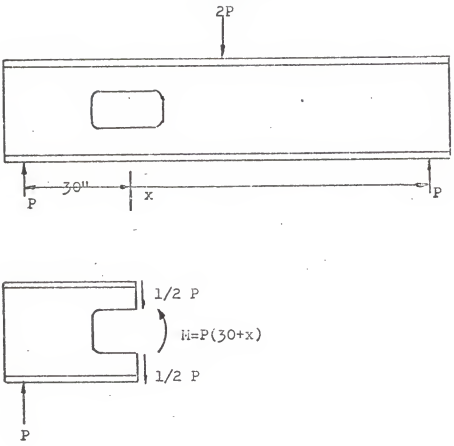

Fig. B1 Schematic View Of Beam And Stresses In Vierendeel Analysis

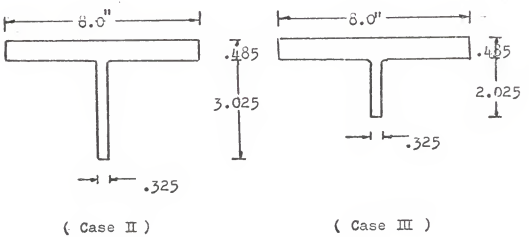

Fig. B2 Dimension Of Tee Sections For Cases II and III

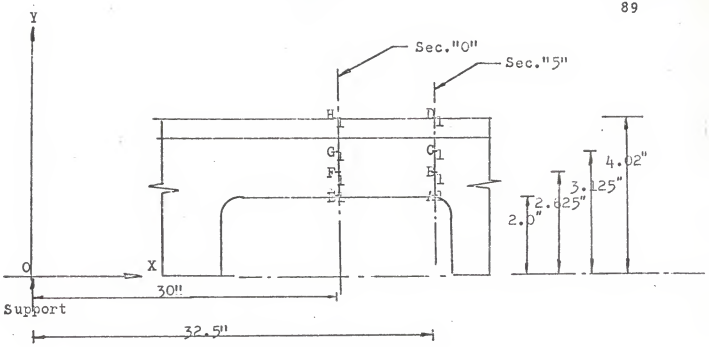

Fig. B3 Coordinate System For The Calculation Of Bending Stress Of Vierendeel Analysis (Case III)

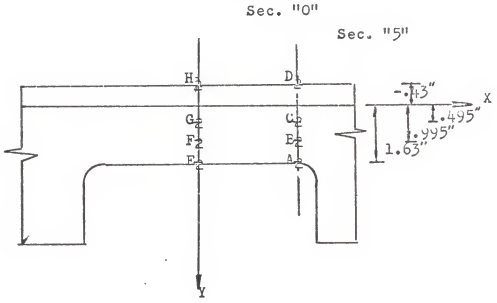

Fig. B4 Coordinate System For The Calculation Of Shearing Stresses Of Vierendeel Analysis (Case III)

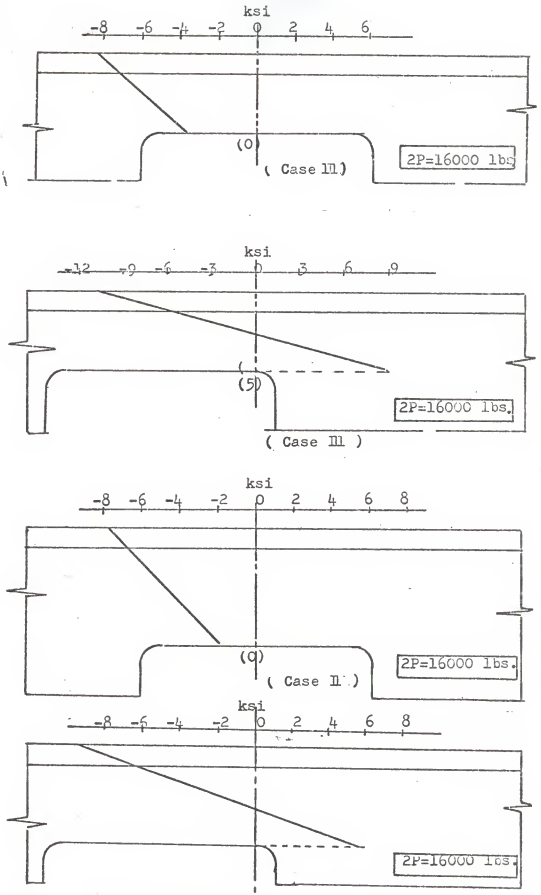

Fig. 5B Stresses Resulting From Vierendeel Analysis

EXPERIMENTAL STUDY OF BEAMS WITH WEB OPENINGS

by

KUO-SHU CHENG

Diploma, Taipei Institute of Technology,
Taiwan, China, 1965

AN ABSTRACT OF A MASTER'S THESIS

submitted in partial fulfillment of the

requirements for the degree

MASTER OF SCIENCE

Department of Civil Engineering

KANSAS STATE UNIVERSITY
Manhattan, Kansas

1969

ABSTRACT

This investigation presents the results of an experimental study of a WF beam (8 WF 35) with a large unreinforced web opening subjected to bending and shear stresses. The purpose of the study was to investigate the stresses in the vicinity of the opening using photostress and electrical strain gage measurements. The results are compared with values calculated by the so-called "Vierendeel Analysis".

The test beam was an ASTM A36 steel WF beam (8 WF 35) with a rectangular web opening at the quarterpoint of the span, and was tested as a simply supported beam with a concentrated load at mid-span. Tests were initially conducted on the beam without a web opening, then with a 2" x 6" rectangular opening and a larger 4" x 6" rectangular opening, and finally the beam was subjected to an ultimate load test. The openings were centered on the centroidal axis of the beam and all corners had 1/2" radius fillets.

The results indicated that the beam with a large unreinforced web opening will have stress concentrations at the corners of the opening, resulting in a non-linear bending stress distribution in a region adjacent to the boundary of the opening. The "Vierendeel Analysis" provided a reasonable prediction of the normal stresses above and below the opening. Finally, it is concluded that an experimental analysis using photostress and strain gage measurements can be quite effective in determining the stresses in a beam with a web opening if proper experimental techniques are used.